Cell Reports

Report

Axis Patterning by BMPs: Cnidarian Network Reveals Evolutionary Constraints

Graphical Abstract

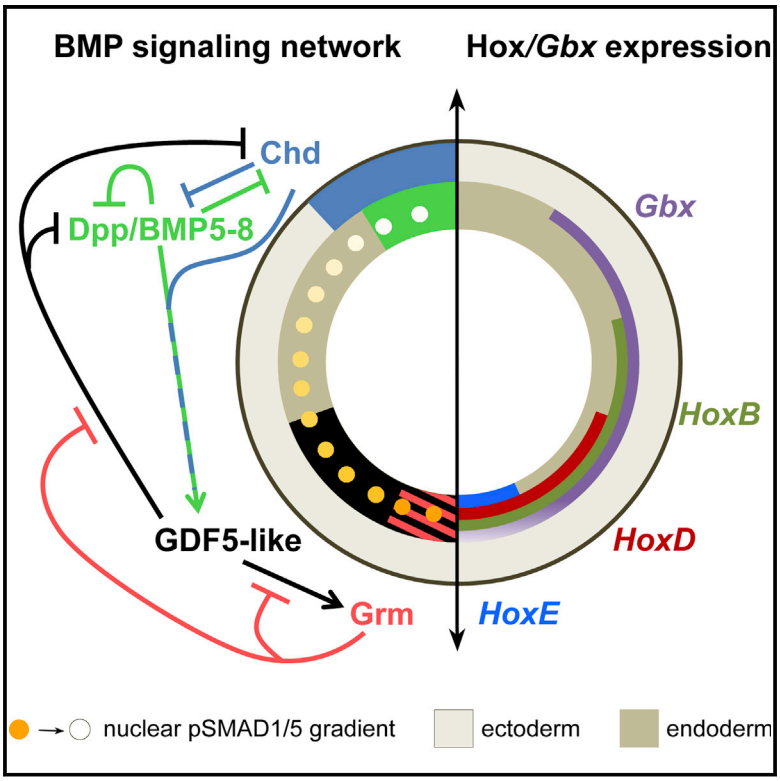

Authors

Grigory Genikhovich, Patrick Fried, ..., Dagmar Iber, Ulrich Technau

Correspondence

ulrich.technau@univie.ac.at

In Brief

Similar to Bilateria, anthozoans possess a secondary directive body axis. Genikhovich et al. examine the bone morphogenetic protein (BMP) signaling network required to compartmentalize the directive axis and regulate staggered Hox gene expression in a sea anemone. Mathematical modeling reveals the constraints guiding the evolution of the axis-forming BMP networks in animals.

Highlights

- A gradient of BMP signaling maintains the directive axis in *Nematostella*
- BMP signaling regulates *Nematostella Hox* genes and patterns the endoderm
- BMP network topology is similar in *Nematostella* and *Xenopus*
- Constraint analysis reveals the evolvability of BMP network components

Accession Numbers

KJ948110

Genikhovich et al., 2015, Cell Reports *10*, 1646–1654
March 17, 2015 ©2015 The Authors
http://dx.doi.org/10.1016/j.celrep.2015.02.035

CellPress

OPEN ACCESS
CellPress

Cell Reports
Report

Axis Patterning by BMPs: Cnidarian Network Reveals Evolutionary Constraints

Grigory Genikhovich,[1] Patrick Fried,[2,3] M. Mandela Prünster,[1] Johannes B. Schinko,[1,5] Anna F. Gilles,[1,5] David Fredman,[1,4] Karin Meier,[2] Dagmar Iber,[2,3] and Ulrich Technau[1,*]

[1]Department for Molecular Evolution and Development, Centre of Organismal Systems Biology, University of Vienna, Althanstraße 14, 1090 Vienna, Austria

[2]Department for Biosystems Science and Engineering, ETH Zurich, Mattenstrasse 26, 4058 Basel, Switzerland

[3]Swiss Institute of Bioinformatics, Mattenstrasse 26, 4058 Basel, Switzerland

[4]Computational Biology Unit, University of Bergen, Thormøhlensgt. 55, 5008 Bergen, Norway

[5]Present address: Comparative Developmental Biology and Regeneration, Institut de Génomique Fonctionnelle de Lyon (IGFL), 32-34 Avenue Tony Garnier, Lyon 69007, France

*Correspondence: ulrich.technau@univie.ac.at

http://dx.doi.org/10.1016/j.celrep.2015.02.035

SUMMARY

BMP signaling plays a crucial role in the establishment of the dorso-ventral body axis in bilaterally symmetric animals. However, the topologies of the bone morphogenetic protein (BMP) signaling networks vary drastically in different animal groups, raising questions about the evolutionary constraints and evolvability of BMP signaling systems. Using loss-of-function analysis and mathematical modeling, we show that two signaling centers expressing different BMPs and BMP antagonists maintain the secondary axis of the sea anemone *Nematostella*. We demonstrate that BMP signaling is required for asymmetric *Hox* gene expression and mesentery formation. Computational analysis reveals that network parameters related to BMP4 and Chordin are constrained both in *Nematostella* and *Xenopus*, while those describing the BMP signaling modulators can vary significantly. Notably, only *chordin*, but not *bmp4* expression needs to be spatially restricted for robust signaling gradient formation. Our data provide an explanation of the evolvability of BMP signaling systems in axis formation throughout Eumetazoa.

INTRODUCTION

Bone morphogenetic protein (BMP) signaling regulates dorso-ventral (DV) axis patterning in Bilateria. Binding of a homo- or heterodimeric BMP ligand to the BMP receptor leads to phosphorylation of SMAD1/5/8, which enters the nucleus together with SMAD4 and regulates transcription of target genes (Plouhinec et al., 2011). Several BMP family molecules, BMP2/4, BMP5-8, ADMP, and Gdf5/6, use this pathway, however, the most prominent members of the family are BMP2/4 and BMP5-8. Signaling is regulated extracellularly by several antagonists, including Chordin, which binds to BMPs and prevents them from binding their receptors (Piccolo et al., 1996). In contrast to other BMP antagonists, Chordin can be cleaved by Tolloid metalloprotease, resulting in the release of active BMP ligand (Piccolo et al., 1997). Thus, Chordin acts as a BMP shuttle diffusing away from Chordin source and promoting signaling at a distance (Plouhinec et al., 2011).

These interactions form a BMP signaling gradient patterning the DV axis in vertebrates and insects, leading to the idea of a common evolutionary origin of the DV axis in Bilateria (Arendt and Nübler-Jung, 1994; De Robertis, 2008). Indeed, in vertebrates and in *Drosophila*, *bmp4* and *chordin* homologs are expressed at the opposite ends of the DV axis (Figure 1A), and the position of the CNS is defined by suppression of BMP signaling, independent of whether the CNS is dorsal, as in vertebrates, or ventral, as in flies. Yet, even within Bilateria, variations regarding expression domains and network topology exist. For example, sea urchin *bmp4* and *chordin* are co-expressed on the same side of the DV axis (Figure 1A; Lapraz et al., 2009), and many molecules were shown to play crucial roles in DV patterning in some phyla but not in others (Inomata et al., 2008, 2013; Jaźwińska et al., 1999; Lee et al., 2006; Reversade and De Robertis, 2005), which raises the question of the ancestral condition in Bilateria. In this respect Cnidaria, the sister group to Bilateria (Hejnol et al., 2009; Philippe et al., 2011), is pivotal for understanding the evolution of key bilaterian traits. Among cnidarians, Anthozoa (corals, sea anemones) encompass bilaterally symmetric animals with a directive axis orthogonal to the oral-aboral axis. Previous work demonstrated that the directive axis of the sea anemone *Nematostella vectensis* is marked by asymmetric expression of BMPs and BMP antagonists (Finnerty et al., 2004; Matus et al., 2006a, 2006b; Rentzsch et al., 2006; Saina et al., 2009), pointing at the possible common evolutionary origin of the directive axis and the bilaterian DV axis.

Surprisingly, expression domains of the *Nematostella* homologs of vertebrate *bmp4* and *chordin*, *NvDpp* and *NvChd*, are not opposed as in vertebrates and insects but become co-localized during gastrulation at the same side of the embryo (Rentzsch et al., 2006), as in sea urchin (Lapraz et al., 2009; Figures 1A and 1B). This symmetry break depends on BMP

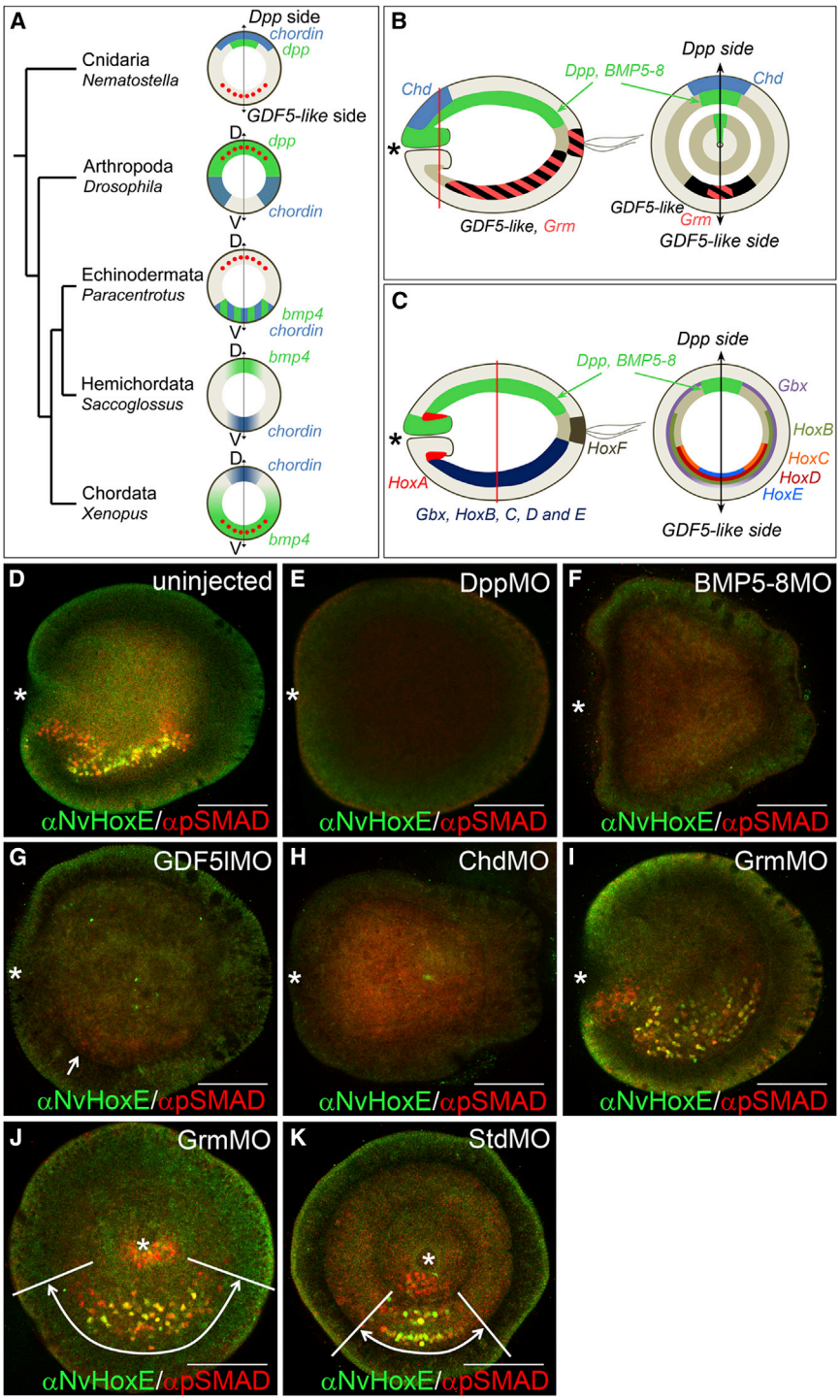

Figure 1. BMP Signaling Is Strongest on *GDF5-like*-Expressing Side of *Nematostella* Embryo

(A) Positions of *chordin* (blue) expression, *bmp4* (green) expression, and BMP signaling domain (red circles) in different animal models.

(B and C) Schematic representation of *NvDpp*, *NvBMP5-8*, *NvGDF5-like*, *NvChd*, *NvGrm*, *NvGbx*, and *Hox* expression domains in planula viewed laterally and orally. Red lines, cutting planes; black double-headed arrows, directive axis; asterisks, blastopore.

(D–K) The αpSMAD1/5 and αNvHoxE antibody staining in control and morphant early planulae, $n > 50$ for each sample; (D–I) lateral views; (J and K) oral views; asterisks, blastopore. (D) αpSMAD1/5-positive nuclei are located on NvHoxE-expressing side. αpSMAD1/5 and αNvHoxE stainings partially overlap. (E–K) αpSMAD1/5 and αNvHoxE in StdMO, ChdMO, GrmMO, GDF5lMO, BMP5-8MO, and DppMO embryos. Staining is absent in DppMO, BMP5-8MO, and ChdMO and suppressed (white arrow) in GDF5lMO (E–H); the domain showing strong staining (white double-headed arrows and white demarcating lines) is narrower in the StdMO than in the GrmMO (J and K).

See also Figure S1.

signaling itself (Saina et al., 2009). Another BMP gene, *NvGDF5-like*, and a gene coding for a BMP antagonist *gremlin* (*NvGrm*) also are expressed asymmetrically in early planula, yet on the opposite side of *NvDpp*, *NvBMP5-8*, and *NvChd* (Figure 1B), suggesting a more complex network (Rentzsch et al., 2006). How such signaling system evolved and what constraints limited its evolutionary divergence is unclear. Here, by a combination of gene knockdown analysis and mathematical modeling, we reveal the functional links and constraints of the BMP signaling network regulating the maintenance of the directive axis in *Nematostella*. Our data provide an explanation for the evolutionary divergence of BMP-dependent axis regulation observed among animals.

RESULTS

BMP Signaling Forms a Gradient along the Directive Axis

Opposing expression of two sets of BMPs and BMP antagonists (*NvDpp/NvBMP5-8/NvChd* and *NvGDF5-like/NvGrm*) along the directive axis makes it difficult to predict how these secreted factors influence one another and where BMP signaling occurs. Using anti-pSMAD1/5 antibody staining as a readout of BMP signaling, we revealed strong nuclear pSMAD1/5 staining on one side of the directive axis in early planula (Figure 1D). Since different BMPs are expressed on different sides of the embryo (Figure 1B; Table S1), and because no morphological landmarks exist, it was unclear where BMP signaling is active along the directive axis. Double in situ hybridization experiments showed that *NvDpp* and a *Hox* gene *NvHoxE* (Figures 1C and S1A; Table S2) are expressed on opposing sides of the directive axis

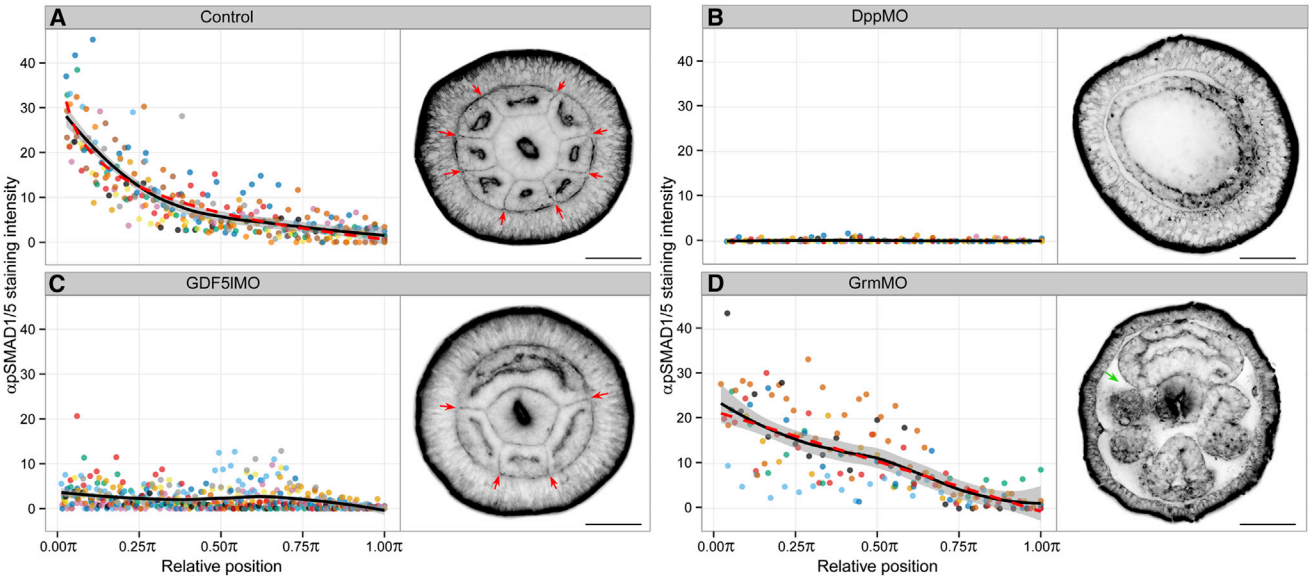

Figure 2. Effect of MO Knockdown on αpSMAD1/5 Staining Gradient and Morphology of Late Planulae

(A–D) Nuclear αpSMAD1/5 staining intensity as a function of relative position of each endodermal nucleus along 180° arc from 0 to π starting at the middle of pSMAD1/5-positive domain (see the Supplemental Experimental Procedures and Figure S2A for details on measuring), described by measurements from multiple embryos (colored points) for Control (n = 12), GrmMO (n = 7), GDF5lMO (n = 10), and DppMO (n = 8). LOESS smoothed curves (black lines) with 99% confidence interval for the mean (shade), and linear model fit of the logarithm of relative position to pSMAD1/5 staining intensity (R^2 = 0.73, dashed red line) for Control embryos and linear model fit of relative position to pSMAD1/5 staining intensity (R^2 = 0.55, dashed red line) for GrmMO embryos. Oral views of corresponding StdMO, DppMO, GDF5lMO, and GrmMO late planulae stained with fluorescent phalloidin are shown next to the graphs (n > 55 for each sample). While StdMO planulae with normal nuclear pSMAD1/5 gradient develop eight mesenteries (red arrows in A), DppMO-injected planulae lacking the pSMAD1/5 gradient do not develop mesenteries at all (B). αpSMAD1/5 staining intensity is suppressed but not absent in the GDF5lMO planulae correlating with the formation of four mesenteries instead of eight (red arrows in C). In GrmMO-treated embryos (D), the average pSMAD1/5 staining intensity is elevated in mid-range positions (see also Figure S2C) and more variable than in Control embryos across the whole range (see also Figure S2D). The endoderm in GrmMO appears compartmentalized but its development is abnormal with extremely thickened mesogloea (green arrow). Scale bars represent 50 μm.
See also Figure S2.

(Finnerty et al., 2004; Ryan et al., 2007). Therefore, we generated an anti-NvHoxE antibody and co-immunostained the embryos with anti-pSMAD1/5 and anti-NvHoxE (Figures 1C and S1). We found that these two epitopes partially co-localized in the same endodermal nuclei on the *NvGDF5-like*-expressing side of the embryo, with additional pSMAD1/5 staining in the pharyngeal ectoderm (Figures 1D and 1K). Thus, the peak of BMP signaling was found at a maximal distance to the source of NvDpp protein.

To assess the role of various BMPs and BMP antagonists in establishing pSMAD1/5 signaling, we performed antisense morpholino (MO)-mediated knockdowns. Nuclear pSMAD1/5 staining was absent in *NvDpp* and *NvBMP5-8* morphants and strongly suppressed in *NvGDF5-like* morphants (Figures 1E–1G), suggesting that all three BMPs from both sides contribute to signaling via pSMAD1/5. The pSMAD1/5 staining also was abolished upon knockdown of *NvChd* (Figure 1H), suggesting that BMP signaling depends on the pro-BMP action of Chordin at a distance. Conversely, in *NvGrm* knockdowns, the pSMAD1/5-positive domain expanded in comparison to embryos injected with standard control morpholino (StdMO) (Figures 1I–1K), suggesting that Gremlin locally restricts BMP signaling. We then quantified pSMAD1/5 staining intensity in endodermal nuclei on confocal sections of control and morphant embryos and showed a BMP signaling gradient along the directive axis, which was abolished upon injection of DppMO, suppressed in GDF5lMO and expanded in GrmMO, with significantly ($p < 0.05$, Wilcoxon exact test) elevated pSMAD1/5 levels at middle positions (Figures 2 and S2B–S2D).

By late planula stage, the anlagen of the eight endodermal folds called mesenteries are formed in *Nematostella*. Phalloidin staining showed that all control late planulae contained eight mesenteries (Figure 2A), whereas no mesenteries formed in DppMO, BMP5-8MO, and ChdMO planulae (Figures 2B, S2E, and S2F). Strikingly, upon knockdown of *NvGDF5-like*, which leads to a much shallower gradient of pSMAD1/5, only four mesenteries were formed (Figure 2C). Knockdown of *NvGrm*, which results in an expanded pSMAD1/5 gradient, led to impaired outgrowth of mesenteries and inflated mesogloea (the normally thin extracellular matrix separating the ectodermal and endodermal layers) (Figure 2D). This demonstrates that BMP signaling is necessary for the formation and positioning of the mesenteries.

Hox Genes Are Regulated by BMP Signaling

In early planula, *NvHoxB*, *NvHoxD*, and *NvHoxE* are expressed endodermally in staggered domains along the directive axis together with *NvGbx*, demarcating the positions of future

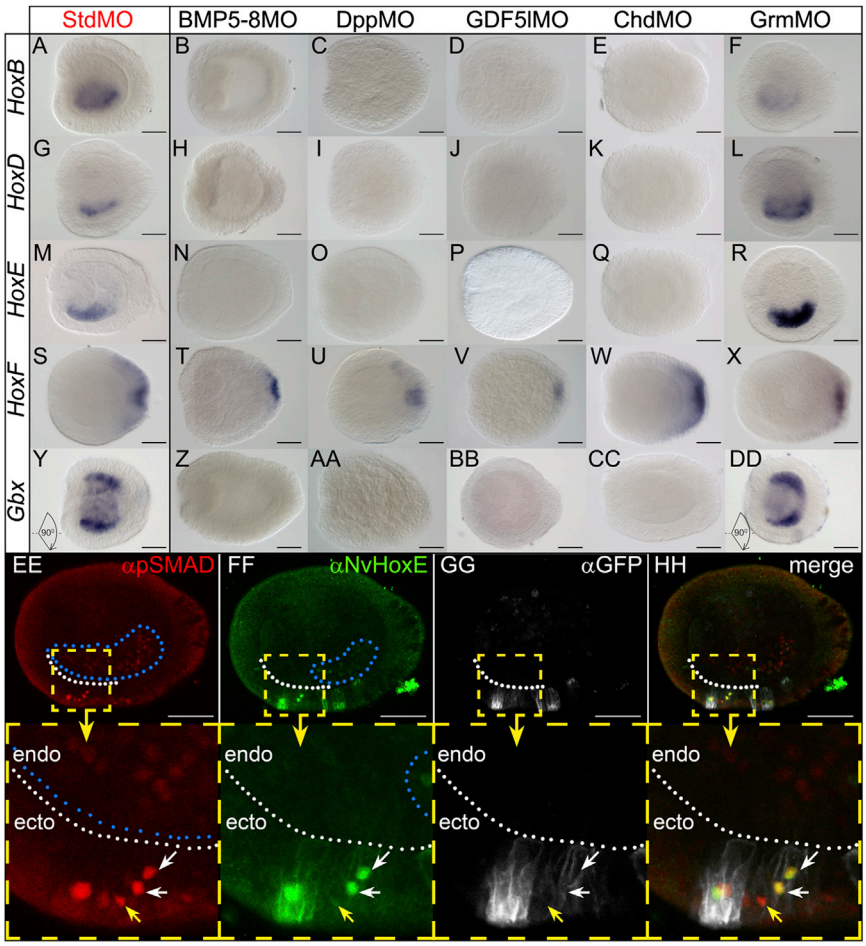

Figure 3. Staggered Endodermal Expression of *Hox* Genes and *NvGbx* Is Regulated by BMP Signaling

(A–DD) Expression of *NvHoxB* (A–F), *NvHoxD* (G–L), *NvHoxE* (M–R), *NvHoxF* (S–X), and *NvGrm* (Y–DD) in StdMO-, BMP5-8MO-, DppMO-, GDF5lMO-, ChdMO-, and GrmMO-injected embryos at early planula stage. Lateral views; oral end to the left. Embryos on (Y) and (DD) are rotated 90° compared to other stained embryos to make bilateral expression of *NvGbx* visible.

(EE–HH) Ectopic expression of $BMPRI_{Q209\,>\,D}$-EGFP in patches of ectodermal cells in 2-day planula results in ectopic activation of NvHoxE protein. (EE) Ectopic pSMAD1/5-positive nuclei in the ectoderm of early planula in addition to endogenous staining in the endoderm (blue dots). (FF) In addition to endogenous αNvHoxE staining (blue dots), ectopic expression is observed in pSMAD1/5-positive ectodermal nuclei. Apart from specific nuclear NvHoxE signal, the secondary anti-rat antibody cross-reacts with mouse anti-GFP antibody staining the $BMPRI_{Q209\,>\,D}$-EGFP fusion protein in the cell membranes. (GG) Anti-GFP antibody detects $BMPRI_{Q209\,>\,D}$-EGFP in cell membranes. Anti-mouse antibody does not cross-react with the rat αNvHoxE, thus no nuclear staining is observed, showing that nuclear staining on (FF) is specific for NvHoxE. (HH) Merged image of (EE–GG). White dots indicate the border between ectoderm and endoderm. White arrows point at two strongly pSMAD1/5-positive ectodermal nuclei in transgenic cells, which also ectopically express NvHoxE. Yellow arrows point at a weakly pSMAD1/5-positive ectodermal nucleus in a transgenic cell, which does not express detectable amounts of NvHoxE. Scale bars represent 50 μm. See also Figure S3.

mesenteries (Ryan et al., 2007; Figures 1C and S1A; Table S2), while *NvHoxF* is expressed in a radially symmetric domain in the aboral ectoderm (Ryan et al., 2007; Figure 1C; Table S2). Whenever pSMAD1/5 staining was abolished, NvHoxE also could not be detected (Figures 1E–1K), suggesting that NvHoxE expression is downstream of BMP signaling.

To test whether other *Hox* genes also might be controlled by BMP signaling, we assessed their expression upon knockdown of BMP network members. We found that the aboral ectodermal expression of *NvHoxF* is not abolished by any of the knockdowns (Figures 3S–3X and S3). However, all endodermally, asymmetrically expressed *Hox* genes, as well as *NvGbx*, are abolished or strongly suppressed in BMP5-8MO, DppMO, GDF5LMO, and ChdMO (Figures 3A–3E, 3G–3K, 3M–3Q, 3Y–3CC, and S3). In contrast, upon knockdown of *NvGrm*, the endodermal *Hox* genes are either barely affected (*NvHoxB*, *NvHoxD*) or enhanced and broadened (*NvHoxE*) (Figures 3F, 3L, 3R, 3X, 3DD, and S3).

To test whether BMP signaling is sufficient to activate Hox gene expression, we overexpressed a constitutively active BMP receptor type I fused C-terminally to EGFP ($BMPRI_{Q209\,>\,D}$-EGFP) in a mosaic fashion in the embryo and assayed for NvHoxE protein. We found that, in addition to the endogenous endodermal domain, NvHoxE protein was detected ectopically in the nuclei of the transgenic ectodermal cells, concurrent with the strong expression of pSMAD1/5 (Figures 3EE–3HH). Together, these data show that BMP signaling is necessary for endodermal *Hox* gene expression and sufficient to induce at least *NvHoxE*. The regulation of axial *Hox* gene expression by BMP signaling is unexpected, as so far the only known upstream regulatory role of BMP signaling on *Hox* genes is the transient and likely indirect activation of *Hox* genes in the non-organizer mesoderm in *Xenopus* (Wacker et al., 2004).

The Topology of the BMP Signaling Network

To understand the regulatory interactions required for maintaining a stable BMP signaling gradient patterning the directive axis in early planulae, we assessed expression of *NvGDF5-like*, *NvBMP5-8*, *NvDpp*, *NvChd*, and *NvGrm* upon knockdown of each of them (Figures 4A and S3).

NvDpp, *NvBMP5-8*, and *NvChd* expression (Figure 4A, images 7, 13, and 19) was restricted to the side of weak BMP signaling (Figures 1B and 1D). MO knockdown of *NvDpp* and *NvBMP5-8* resulted in upregulation and radialization of *NvDpp*, *NvBMP5-8*, and *NvChd* expression (Figure 4A, images 8–9, 14–15, and 20–21), suggesting that strong BMP signaling suppresses transcription of these genes. In contrast, *NvGDF5-like*

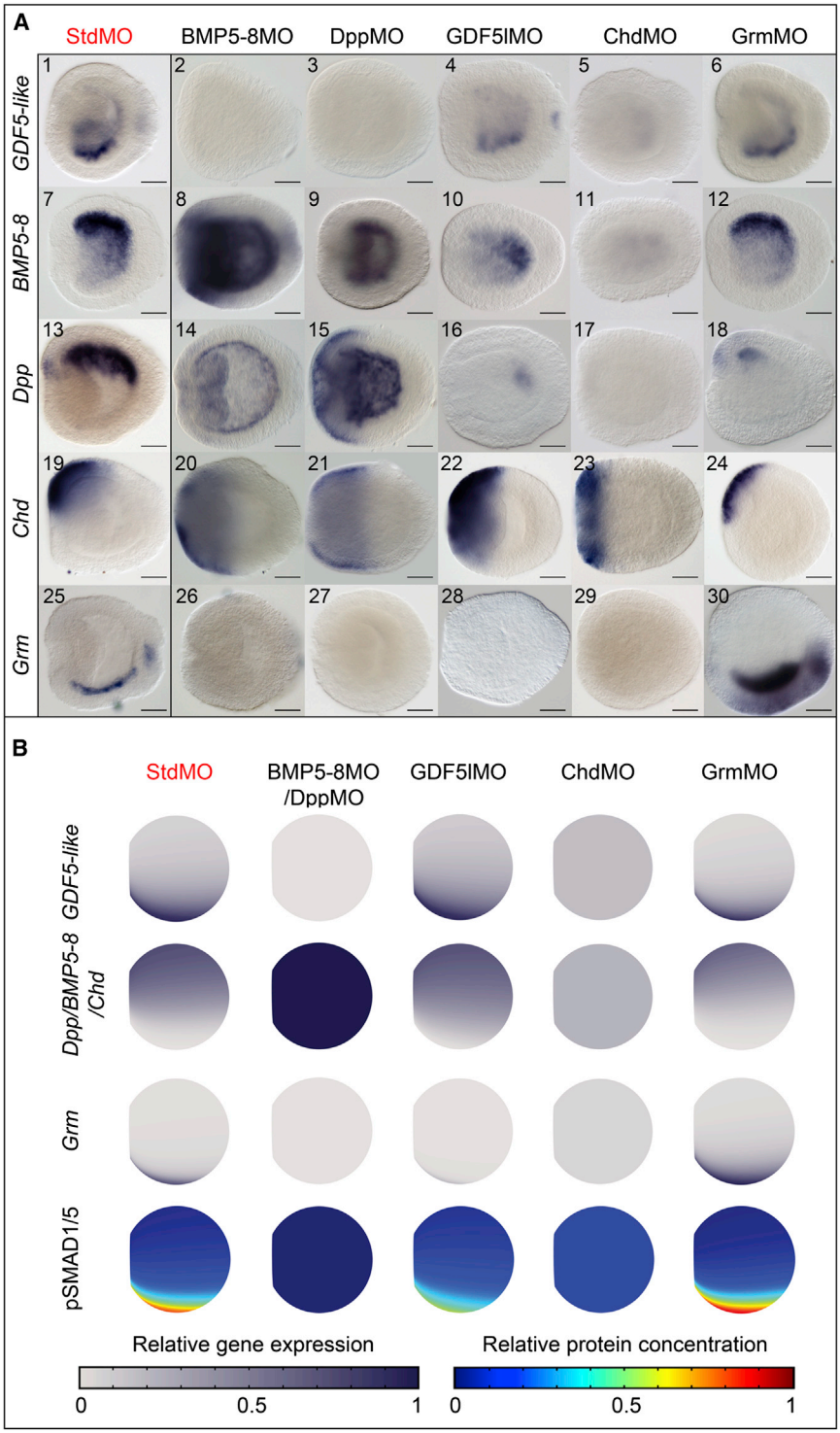

Figure 4. Maintenance of the Directive Axis in *Nematostella*

(A) Expression analysis of network components in morphant early planulae; lateral views, oral end is to the left. Scale bars represent 50 μm.

(B) Mathematical model correctly predicts expression patterns of all genes shown in (A) (color code as in ISH), as well as pSMAD1/5 localization (shown as heat maps) in the knockdowns. All expression patterns and pSMAD1/5 staining patterns are plotted onto mesogloea and shown as 2D projections of a 3D structure. Expression domains of *NvDpp*/*NvBMP5-8*/*NvChd*, although not identical, strongly overlap when plotted onto mesogloea. In the model they are controlled by the same mathematical expression and thus plotted together.

See also Figures S3 and S4.

expression was restricted to the side of maximal pSMAD1/5 (Figures 1B, 1D, and 4A, image 1). *NvGDF5-like* transcription in early planula is regulated by signaling via NvDpp and NvBMP5-8 as it was absent in the BMP5-8MO and the DppMO (Figure 4A, images 2–3). Chordin appeared to be pivotal for both the restriction of *NvDpp*, *NvBMP5-8*, and its own expression to an asymmetric domain on one side of the directive axis and for the signaling via NvDpp and NvBMP5-8 at the opposite side of the directive axis. In ChdMO, *NvDpp* and *NvBMP5-8* expression was suppressed (Figure 4A, images 11 and 17) and *NvChd* expression was radialized (Figure 4A, image 23). At the same time, the NvDpp and NvBMP5-8 signaling target *NvGDF5-like* on the opposite side was abolished (Figure 4A, image 5). These data suggest that Chordin locally antagonizes BMP signaling by binding NvDpp and NvBMP5-8, but facilitates their function at a distance acting as a shuttle molecule, similar to the situation in *Drosophila* (Eldar et al., 2002) and *Xenopus* (Ben-Zvi et al., 2008). Given that *NvDpp* and *NvBMP5-8* are co-expressed in *Nematostella* and their MO phenotypes are indistinguishable (Saina et al., 2009; Figure 4A), it is likely that NvDpp and NvBMP5-8 heterodimerize. Disappearance of the *NvDpp* and *NvBMP5-8* expression in ChdMO also suggests that a low level of BMP signaling facilitated by NvChd might be required for the proper expression of *NvDpp* and *NvBMP5-8*.

Like *NvGDF5-like*, BMP antagonist *NvGrm* is expressed opposite to *NvDpp* (Rentzsch et al., 2006; Figure 4A, image 25), and *NvGrm* expression was absent in GDF5LMO, DppMO, BMP5-8MO, and ChdMO (Figure 4A, images 26–29). However, *NvGDF5-like* knockdowns still showed *NvBMP5-8* and *NvDpp* expression (Figure 4A, images 10 and 16), but lacked *NvGrm* expression (Figure 4A, image 28), suggesting that in early planula *NvGrm* is induced only by

NvGDF5-like signaling. *NvGDF5-like* expression is not affected in GrmMO (Figure 4A, image 6), suggesting that NvGrm does not antagonize the NvDpp/NvBMP5-8 complex as otherwise NvGrm knockdown would lead to an upregulation of *NvGDF5-like*. Instead, NvGrm appears to antagonize NvGDF5-like signaling, as *NvGrm* was strongly upregulated in GrmMO (Figure 4A, image 30), suggesting enhanced NvGDF5-like signaling. NvGDF5-like signaling does not regulate *NvGDF5-like* expression as neither in GDF5LMO nor in GrmMO was *NvGDF5-like* expression affected (Figure 4A, images 4 and 6).

NvGDF5-like and *NvGrm* knockdowns indicate the contribution of NvGDF5-like to the formation of the weak BMP signaling on the *NvDpp*-expressing side of the planula. Both GDF5LMO and GrmMO resulted in a reduction of the unilateral *NvDpp*-expressing domain to the aboral or oral endoderm, respectively (Figure 4A, images 16 and 18). *NvChd* expression is suppressed by NvGDF5-like signaling, since the *NvChd* expression domain was radially expanded in GDF5IMO and not in GrmMO (Figure 4A, images 22 and 24).

Modeling Reveals Constraints of the Network

Given the complexity of the network interactions, we resorted to mathematical modeling to reveal functional constraints on the components of the BMP network. We used our loss-of-function data to generate a 3D computational model of BMP signaling-dependent maintenance of the directive axis in *Nematostella*. Our results suggest that Chordin acts as a shuttle for the Dpp/BMP5-8 heterodimer, similar to the situation in *Drosophila* and *Xenopus* during DV patterning (Ben-Zvi et al., 2008; Eldar et al., 2002; Iber and Gaglia, 2007; Mizutani et al., 2005). A mathematical model for BMP ligand shuttling by Mizutani and coworkers focuses on the core part of the regulatory network and reproduces the kinetics of the maintenance of the BMP signaling in *Drosophila* correctly (Iber and Gaglia, 2007; Mizutani et al., 2005). To test whether similar rules also would apply to a non-bilaterian, we adapted the model to *Nematostella* (Figure S4A, black part) by including NvGDF5-like and NvGrm (Figure S4A, colored part) in addition to NvDpp, NvBMP5-8, and NvChd and by removing Twisted gastrulation (Tsg), as *Tsg* is absent from the *Nematostella* genome (Putnam et al., 2007). Our aim was to include these components with the least alterations to the *Drosophila* model in a way that all key experimental observations in control and MO experiments in *Nematostella* could be reproduced and thus generate a minimal viable model of BMP signaling maintenance in *Nematostella* after symmetry break (see the Supplemental Experimental Procedures for details).

According to the core model (Figure S4A, black part), the diffusible NvDpp/NvBMP5-8 heterodimer (termed BMP in the schemes) can either form an inactive diffusible complex with NvChd, or bind the BMP receptor to form an active signaling complex and undergo degradation (for details see the Supplemental Experimental Procedures). As in other systems, NvChd, when bound to the NvDpp/NvBMP5-8 ligand, is cleaved by ubiquitously endodermally expressed Tolloid (Matus et al., 2006b) to release the active BMP heterodimer. After the simulation start, shuttling of NvDpp/NvBMP5-8 by Chordin rapidly results in a stable BMP signaling gradient with a maximum opposite to the *NvChd* expression domain (Figure S4), consistent with the experimentally observed pSMAD1/5 distribution. BMP signaling then represses *NvChd* expression (Figure S4A, red dashed lines), maintaining the restricted expression patterns. The initial restriction on *NvChd* expression needs to be imposed for only 15 min in the model. Thereafter, the simulation reproduces all important aspects of the expression of *NvDpp*, *NvBMP5-8*, *NvGDF5-like*, *NvChd*, and *NvGrm*, as well as the location of the BMP signaling domain in the wild-type and the knockdowns (Figures 4B and S4), confirming the role of each of the BMPs and the BMP antagonists in maintaining and shaping the pSMAD1/5 gradient. Thus, we conclude that the deduced topology of the *Nematostella* BMP network (Figure 5A) is consistent with the experimental data.

To assess the sensitivity of the signaling network to perturbation, we systematically increased and decreased all 31 model parameters individually until the model failed to reproduce asymmetric BMP signaling (Figures 5F and S5A). In line with the results of the knockdowns (Figures 3A–3F), many of the parameters linked to NvDpp/NvBMP5-8 and NvChd were heavily constrained, while those related to NvGDF5-like and NvGrm could vary widely without destroying the asymmetric BMP signaling pattern (Figures 5F and S5A).

To test whether a division into constrained core components and unconstrained modulators might represent a conserved evolutionary feature of axis-forming BMP signaling networks, we adapted the model to describe the BMP network regulating DV patterning in frog embryos. As for *Nematostella*, our minimal viable model describing the *Xenopus* BMP network using a subset of the components (for details see the Supplemental Experimental Procedures) reproduced all key aspects of normal expression as well as known loss-of-function and overexpression phenotypes of BMP4/BMP7, ADMP/BMP2, Chordin, SMAD6/7, and BAMBI (Khokha et al., 2005; Paulsen et al., 2011; Reversade and De Robertis, 2005; Figures S4B and S4J). The sensitivity analysis demonstrated that in frog, like in *Nematostella*, there is a conserved core of the network with strongly constrained parameters (BMPs, Chordin, Tolloid) and peripheral weakly constrained signaling modulators, such as BAMBI and SMAD6/7 (Figures 5F, 5G, and S5).

DISCUSSION

Similar to Bilateria, anthozoans have a second body axis specified by BMP signaling (Saina et al., 2009; Leclère and Rentzsch, 2014). We have shown that various BMPs and BMP antagonists from opposing sides of the *Nematostella* larva contribute to the maintenance of nuclear pSMAD1/5 gradient along the directive axis. This could be interpreted as evidence for common evolutionary origin of the directive and DV axis and loss of bilaterality in medusozoan cnidarians, such as hydroids and jellyfish. The deduced topology of the BMP network maintaining the directive axis in *Nematostella* appears to be remarkably similar to the one described for the DV-patterning network in *Xenopus* (Reversade and De Robertis, 2005; Zakin and De Robertis, 2010; Figures 5A and 5B). However, striking differences in the BMP networks exist between Bilateria and Cnidaria: (1) conserved molecules occupy different positions in the network and there is a positive-versus-negative feedback loop of BMP4/BMP5-8 on their

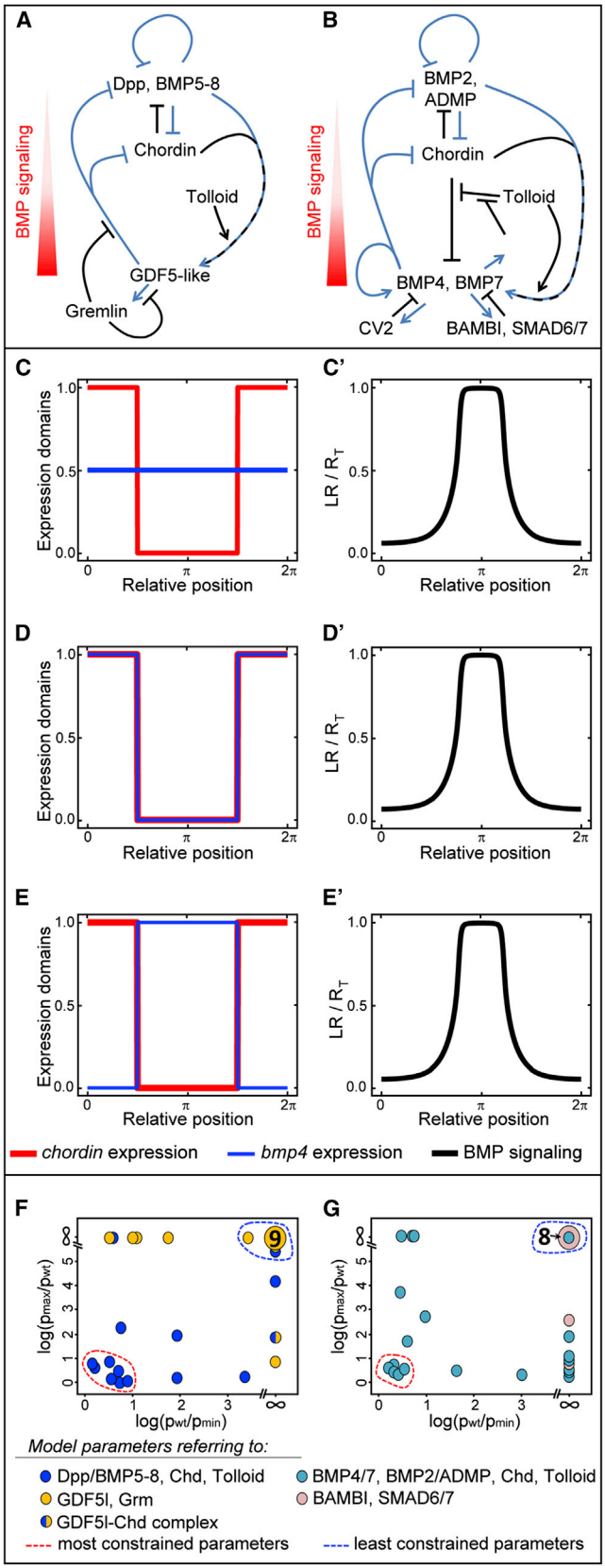

Figure 5. Strongly Constrained Core Interactions and Weakly Constrained Modulators of the BMP Signaling System

(A and B) *Nematostella* directive axis network (A) compared to the DV network in *Xenopus* (B). Blue lines represent transcriptional regulation downstream of BMP signaling and black lines represent protein-protein interactions (putative in case of *Nematostella*). *Xenopus* network is modified after (De Robertis and Colozza, 2013; Paulsen et al., 2011). Overlaid blue and black lines represent shuttle function of Chordin.

(C–E) Restricted *chordin* expression domain (red curves on the left plots) results in BMP signaling on the opposite side of the embryo (relative concentration of BMP ligand-receptor complexes shown as black curves on C′–E′) independent of *bmp4* expression localization (blue curve). *bmp4* can be expressed uniformly (C), on the *chordin* side (D), or opposite to it (E). The x axis is normalized with respect to maximal domain length (shown as 2π since the embryo is spherical), and the y axis shows the ratio of ligand-bound receptors (LR) with respect to total receptor concentration (R_T).

(F and G) Constrained core regulators versus weakly constrained modulators of BMP signaling in *Nematostella* (F) and *Xenopus* (G).

(F) Many parameters describing production, function, and turnover of NvDpp/NvBMP5-8 and NvChd (blue circles) are strongly constrained, while most of the parameters describing production, function, and turnover of NvGDF5-like and NvGrm (orange circles) are weakly constrained. Large orange circle with a 9 corresponds to nine unconstrained parameters related to NvGDF5-like and NvGrm.

(G) Many parameters describing production, function, and turnover of frog BMP4/BMP7, ADMP/BMP2, Chordin, and Tolloid (teal circles) are strongly constrained, while most of the parameters describing production, function, and turnover of BAMBI and SMAD6/7 (pink circles) are weakly constrained. Large pink circle with an 8 corresponds to eight unconstrained parameters related to BAMBI and SMAD6/7. Fold of possible increase of parameter values (log scale) is plotted on the y axis, and fold of possible decrease of parameter values (log scale) is plotted on the x axis. (For details see the Supplemental Experimental Procedures and Figure S5.)

See also Figure S5.

own expression; (2) the involvement of Gdf5 and Gremlin homologs in the initial axis specification, although not unique, is very uncommon in Bilateria (Kuo and Weisblat, 2011; Sidi et al., 2003); and (3) instead of positioning the CNS, in *Nematostella*, the gradient of BMP signaling is used to specify and position the mesenteries and regulate staggered Hox and *Gbx* gene expression in the endoderm. This link of an early BMP gradient and staggered Hox gene expression is uncommon among Bilateria, where Hox genes are a hallmark of patterning the anterior-posterior axis, but not the DV axis. All these differences make homology assumptions of the cnidarian and bilaterian axes problematic.

Combination of gene function analysis and mathematical modeling allows insights into how BMP signaling networks evolved in different animals. One of the obvious differences in the organization of the BMP signaling systems during secondary body-axis patterning in different organisms is the relative location of the *bmp4* and *chordin* expression domains. While in Bilateria *bmp4* and *chordin* are typically expressed on opposing ends of the DV axis (De Robertis, 2008), they are co-expressed in *Nematostella* (Rentzsch et al., 2006) and sea urchin (Lapraz et al., 2009), raising questions about the ancestral mode of *bmp4* and *chordin* expression in Bilateria (Figure 1A). Our 1D computational analysis of differently positioned *bmp4* and *chordin* expression domains reveals, however, that only the spatial restriction of *chordin* expression is crucial, while the

BMP expression domain can vary; BMP signaling maximum always is located opposite to the *chordin* expression domain independent of the *bmp4* expression pattern if shuttling is at work (Figures 5C–5E′). This suggests that there is no selection pressure on the localization of *bmp4*, as long as *chordin* expression is restricted. Support for this conclusion comes from experiments in *Drosophila* showing that the BMP signaling domain is defined solely by *Sog* expression (Wang and Ferguson, 2005), and in *Nematostella* demonstrating that ChdMO injected into one half of the embryo always leads to the formation of the pSMAD1/5-positive domain on the injection side; i.e., where Chordin protein is inactive (Leclère and Rentzsch, 2014).

Sensitivity analysis of our model demonstrated that, consistent with the knockdown phenotypes, the parameters describing production and turnover of NvDpp/NvBMP5-8 and NvChd, which are required for generating the BMP signaling gradient, were strongly constrained (Figures 5F and S5A), while those describing NvGDF5-like and NvGrm, which work as modulators of the BMP signaling, could vary widely (Figures 5F and S5A). Modeling frog BMP signaling network, based on the same principles of ligand shuttling, showed that the same logic of having highly constrained core components and weakly constrained modulators of the BMP signaling also applied here and thus might be a common theme throughout animal evolution (Figures 5G and S5B). An important difference between the *Xenopus* and *Nematostella* networks is that the frog system appears to be more robust due to partial redundancy of the BMP ligands. Different constraints on members of the BMP network give clues as to why BMP signaling modulators seem to be exchanged easily during evolution in various animals, while the involvement of the core components, BMP4 and Chordin, is conserved except for a few known cases, primarily in animals with highly deterministic development like leeches, ascidians, and nematodes (Kuo and Weisblat, 2011; Lemaire, 2009; Patterson and Padgett, 2000), but also in the wasp *Nasonia* (Özüak et al., 2014). In this respect, investigating the DV-patterning mechanism in molluscs, which develop similar to annelids but, unlike annelids, have retained *chordin* in their genomes, will be particularly interesting.

In summary, we deciphered the logic of the BMP signaling network maintaining the secondary body axis in a non-bilaterian species, the sea anemone *Nematostella vectensis*, and demonstrated an unexpected link between BMP signaling and staggered Hox gene expression. Mathematical modeling showed that the spatial restriction of *chordin* expression as well as the production and turnover of the core components of the network appear to be the factors crucial for the functional BMP signaling system in many of the studied Eumetazoa. Since the selection pressure is on the generation of robust signaling gradients, the variety of different network topologies primarily is constrained by the biochemical qualities of the core network components. We conclude that a few key constraints under strong selection pressure keep crucial parameters constant over hundreds of millions of years of separation, while less constrained modulators are added or removed during the evolution of the BMP signaling network, thus generating the diversity of different BMP signaling networks observed in animals.

EXPERIMENTAL PROCEDURES

Animal Culture and Microinjection

Animals were kept and gametogenesis was induced as described (Genikhovich and Technau, 2009a). Antisense MO oligonucleotides (Gene Tools) against *NvDpp*, *NvBMP5-8*, *NvGDF5-like*, *NvChd*, and *NvGrm* were injected into fertilized eggs. For MO sequences, concentrations, and specificity tests as well as for the details on generating the constitutively active *Nematostella* BMPRI, see the Supplemental Experimental Procedures.

Antibody Staining, Phalloidin Staining, and In Situ Hybridization

Rabbit anti-Phospho-Smad1 (Ser463/465)/Smad5 (Ser463/465)/Smad8 (Ser426/428) (Cell Signaling, 9511), rat anti-NvHoxE, rabbit anti-GFP (Abcam, ab290), and mouse anti-GFP (Life Technologies, A11120) were used for the experiments. Intensity of αpSMAD1/5 staining was quantified on 16-bit images of confocal optical sections (oral views) of early morphant and control planulae stained with DAPI and αpSMAD1/5. For F-actin staining, Alexa Fluor 488 phalloidin (Life Technologies, A12379) was used. For the details on raising the anti-NvHoxE antibody, the antibody staining protocol, and pSMAD1/5 gradient quantification, see the Supplemental Experimental Procedures. In situ hybridization was performed as described previously (Genikhovich and Technau, 2009b). For double in situ, the staining was developed as in Denker et al., 2008.

Mathematical Modeling

Details on the mathematical modeling are presented in the Supplemental Experimental Procedures.

ACCESSION NUMBERS

The NvBMPRI sequence has been deposited to the GenBank and is available under accession number KJ948110.

SUPPLEMENTAL INFORMATION

Supplemental Information includes Supplemental Experimental Procedures, five figures, and two tables and can be found with this article online at http://dx.doi.org/10.1016/j.celrep.2015.02.035.

AUTHOR CONTRIBUTIONS

G.G. and U.T. designed experiments. G.G., M.M.P, J.B.S., and A.F.G. performed experiments. G.G. analyzed data. P.F., K.M., and D.I. did mathematical modelling. D.F. performed statistical analysis of gradient data. G.G., U.T., D.I., and P.F. wrote the paper.

ACKNOWLEDGMENTS

We thank the Core Imaging Facility of the Faculty of Life Sciences; Stefanie Wienkoop for performing tandem mass spectrometry (MS/MS) of NvHoxE; Simon Weinberger for working on the antibody staining protocol; Yehu Moran, Eduard Renfer, Andy Aman, and Lucas Leclère for technical advice; Eduard Renfer and Sandra Laufer for isolating β-actin promoter; Patrick Steinmetz, Yehu Moran, and Andy Aman for critically reading the manuscript; and Fabian Rentzsch for sharing unpublished data. This work was funded by grants of the Austrian Science Foundation FWF P22717 (to U.T.) and P26962 (to G.G.) and the EU-ITN EVONET (215781) to U.T.

Received: June 23, 2014
Revised: December 17, 2014
Accepted: February 13, 2015
Published: March 12, 2015

REFERENCES

Arendt, D., and Nübler-Jung, K. (1994). Inversion of dorsoventral axis? Nature *371*, 26.

Ben-Zvi, D., Shilo, B.Z., Fainsod, A., and Barkai, N. (2008). Scaling of the BMP activation gradient in Xenopus embryos. Nature *453*, 1205–1211.

De Robertis, E.M. (2008). Evo-devo: variations on ancestral themes. Cell *132*, 185–195.

De Robertis, E.M., and Colozza, G. (2013). Development: scaling to size by protease inhibition. Curr. Biol. *23*, R652–R654.

Denker, E., Manuel, M., Leclère, L., Le Guyader, H., and Rabet, N. (2008). Ordered progression of nematogenesis from stem cells through differentiation stages in the tentacle bulb of Clytia hemisphaerica (Hydrozoa, Cnidaria). Dev. Biol. *315*, 99–113.

Eldar, A., Dorfman, R., Weiss, D., Ashe, H., Shilo, B.Z., and Barkai, N. (2002). Robustness of the BMP morphogen gradient in Drosophila embryonic patterning. Nature *419*, 304–308.

Finnerty, J.R., Pang, K., Burton, P., Paulson, D., and Martindale, M.Q. (2004). Origins of bilateral symmetry: Hox and dpp expression in a sea anemone. Science *304*, 1335–1337.

Genikhovich, G., and Technau, U. (2009a). In situ hybridization of starlet sea anemone (Nematostella vectensis) embryos, larvae, and polyps. Cold Spring Harb Protoc *2009*, t5282.

Genikhovich, G., and Technau, U. (2009b). Induction of spawning in the starlet sea anemone Nematostella vectensis, in vitro fertilization of gametes, and dejellying of zygotes. Cold Spring Harb Protoc *2009*, t5281.

Hejnol, A., Obst, M., Stamatakis, A., Ott, M., Rouse, G.W., Edgecombe, G.D., Martinez, P., Baguñà, J., Bailly, X., Jondelius, U., et al. (2009). Assessing the root of bilaterian animals with scalable phylogenomic methods. Proc. Biol. Sci. *276*, 4261–4270.

Iber, D., and Gaglia, G. (2007). The mechanism of sudden stripe formation during dorso-ventral patterning in Drosophila. J. Math. Biol. *54*, 179–198.

Inomata, H., Haraguchi, T., and Sasai, Y. (2008). Robust stability of the embryonic axial pattern requires a secreted scaffold for chordin degradation. Cell *134*, 854–865.

Inomata, H., Shibata, T., Haraguchi, T., and Sasai, Y. (2013). Scaling of dorsal-ventral patterning by embryo size-dependent degradation of Spemann's organizer signals. Cell *153*, 1296–1311.

Jaźwińska, A., Kirov, N., Wieschaus, E., Roth, S., and Rushlow, C. (1999). The Drosophila gene brinker reveals a novel mechanism of Dpp target gene regulation. Cell *96*, 563–573.

Khokha, M.K., Yeh, J., Grammer, T.C., and Harland, R.M. (2005). Depletion of three BMP antagonists from Spemann's organizer leads to a catastrophic loss of dorsal structures. Dev. Cell *8*, 401–411.

Kuo, D.H., and Weisblat, D.A. (2011). A new molecular logic for BMP-mediated dorsoventral patterning in the leech Helobdella. Curr. Biol. *21*, 1282–1288.

Lapraz, F., Besnardeau, L., and Lepage, T. (2009). Patterning of the dorsal-ventral axis in echinoderms: insights into the evolution of the BMP-chordin signaling network. PLoS Biol. *7*, e1000248.

Leclère, L., and Rentzsch, F. (2014). RGM regulates BMP-mediated secondary axis formation in the sea anemone Nematostella vectensis. Cell Rep. *9*, 1921–1930.

Lee, H.X., Ambrosio, A.L., Reversade, B., and De Robertis, E.M. (2006). Embryonic dorsal-ventral signaling: secreted frizzled-related proteins as inhibitors of tolloid proteinases. Cell *124*, 147–159.

Lemaire, P. (2009). Unfolding a chordate developmental program, one cell at a time: invariant cell lineages, short-range inductions and evolutionary plasticity in ascidians. Dev. Biol. *332*, 48–60.

Matus, D.Q., Pang, K., Marlow, H., Dunn, C.W., Thomsen, G.H., and Martindale, M.Q. (2006a). Molecular evidence for deep evolutionary roots of bilaterality in animal development. Proc. Natl. Acad. Sci. USA *103*, 11195–11200.

Matus, D.Q., Thomsen, G.H., and Martindale, M.Q. (2006b). Dorso/ventral genes are asymmetrically expressed and involved in germ-layer demarcation during cnidarian gastrulation. Curr. Biol. *16*, 499–505.

Mizutani, C.M., Nie, Q., Wan, F.Y., Zhang, Y.T., Vilmos, P., Sousa-Neves, R., Bier, E., Marsh, J.L., and Lander, A.D. (2005). Formation of the BMP activity gradient in the Drosophila embryo. Dev. Cell *8*, 915–924.

Özüak, O., Buchta, T., Roth, S., and Lynch, J.A. (2014). Ancient and diverged TGF-β signaling components in Nasonia vitripennis. Dev. Genes Evol. *224*, 223–233.

Patterson, G.I., and Padgett, R.W. (2000). TGF beta-related pathways. Roles in Caenorhabditis elegans development. Trends Genet. *16*, 27–33.

Paulsen, M., Legewie, S., Eils, R., Karaulanov, E., and Niehrs, C. (2011). Negative feedback in the bone morphogenetic protein 4 (BMP4) synexpression group governs its dynamic signaling range and canalizes development. Proc. Natl. Acad. Sci. USA *108*, 10202–10207.

Philippe, H., Brinkmann, H., Copley, R.R., Moroz, L.L., Nakano, H., Poustka, A.J., Wallberg, A., Peterson, K.J., and Telford, M.J. (2011). Acoelomorph flatworms are deuterostomes related to Xenoturbella. Nature *470*, 255–258.

Piccolo, S., Sasai, Y., Lu, B., and De Robertis, E.M. (1996). Dorsoventral patterning in Xenopus: inhibition of ventral signals by direct binding of chordin to BMP-4. Cell *86*, 589–598.

Piccolo, S., Agius, E., Lu, B., Goodman, S., Dale, L., and De Robertis, E.M. (1997). Cleavage of Chordin by Xolloid metalloprotease suggests a role for proteolytic processing in the regulation of Spemann organizer activity. Cell *91*, 407–416.

Plouhinec, J.L., Zakin, L., and De Robertis, E.M. (2011). Systems control of BMP morphogen flow in vertebrate embryos. Curr. Opin. Genet. Dev. *21*, 696–703.

Putnam, N.H., Srivastava, M., Hellsten, U., Dirks, B., Chapman, J., Salamov, A., Terry, A., Shapiro, H., Lindquist, E., Kapitonov, V.V., et al. (2007). Sea anemone genome reveals ancestral eumetazoan gene repertoire and genomic organization. Science *317*, 86–94.

Rentzsch, F., Anton, R., Saina, M., Hammerschmidt, M., Holstein, T.W., and Technau, U. (2006). Asymmetric expression of the BMP antagonists chordin and gremlin in the sea anemone Nematostella vectensis: implications for the evolution of axial patterning. Dev. Biol. *296*, 375–387.

Reversade, B., and De Robertis, E.M. (2005). Regulation of ADMP and BMP2/4/7 at opposite embryonic poles generates a self-regulating morphogenetic field. Cell *123*, 1147–1160.

Ryan, J.F., Mazza, M.E., Pang, K., Matus, D.Q., Baxevanis, A.D., Martindale, M.Q., and Finnerty, J.R. (2007). Pre-bilaterian origins of the Hox cluster and the Hox code: evidence from the sea anemone, Nematostella vectensis. PLoS ONE *2*, e153.

Saina, M., Genikhovich, G., Renfer, E., and Technau, U. (2009). BMPs and chordin regulate patterning of the directive axis in a sea anemone. Proc. Natl. Acad. Sci. USA *106*, 18592–18597.

Sidi, S., Goutel, C., Peyriéras, N., and Rosa, F.M. (2003). Maternal induction of ventral fate by zebrafish radar. Proc. Natl. Acad. Sci. USA *100*, 3315–3320.

Wacker, S.A., McNulty, C.L., and Durston, A.J. (2004). The initiation of Hox gene expression in Xenopus laevis is controlled by Brachyury and BMP-4. Dev. Biol. *266*, 123–137.

Wang, Y.C., and Ferguson, E.L. (2005). Spatial bistability of Dpp-receptor interactions during Drosophila dorsal-ventral patterning. Nature *434*, 229–234.

Zakin, L., and De Robertis, E.M. (2010). Extracellular regulation of BMP signaling. Curr. Biol. *20*, R89–R92.

Cell Reports

Supplemental Information

Axis Patterning by BMPs: Cnidarian Network Reveals Evolutionary Constraints

Grigory Genikhovich, Patrick Fried, M. Mandela Prünster, Johannes B. Schinko, Anna F. Gilles, David Fredman, Karin Meier, Dagmar Iber, and Ulrich Technau

Supplemental Figures

Figure S1- related to Figure 1.

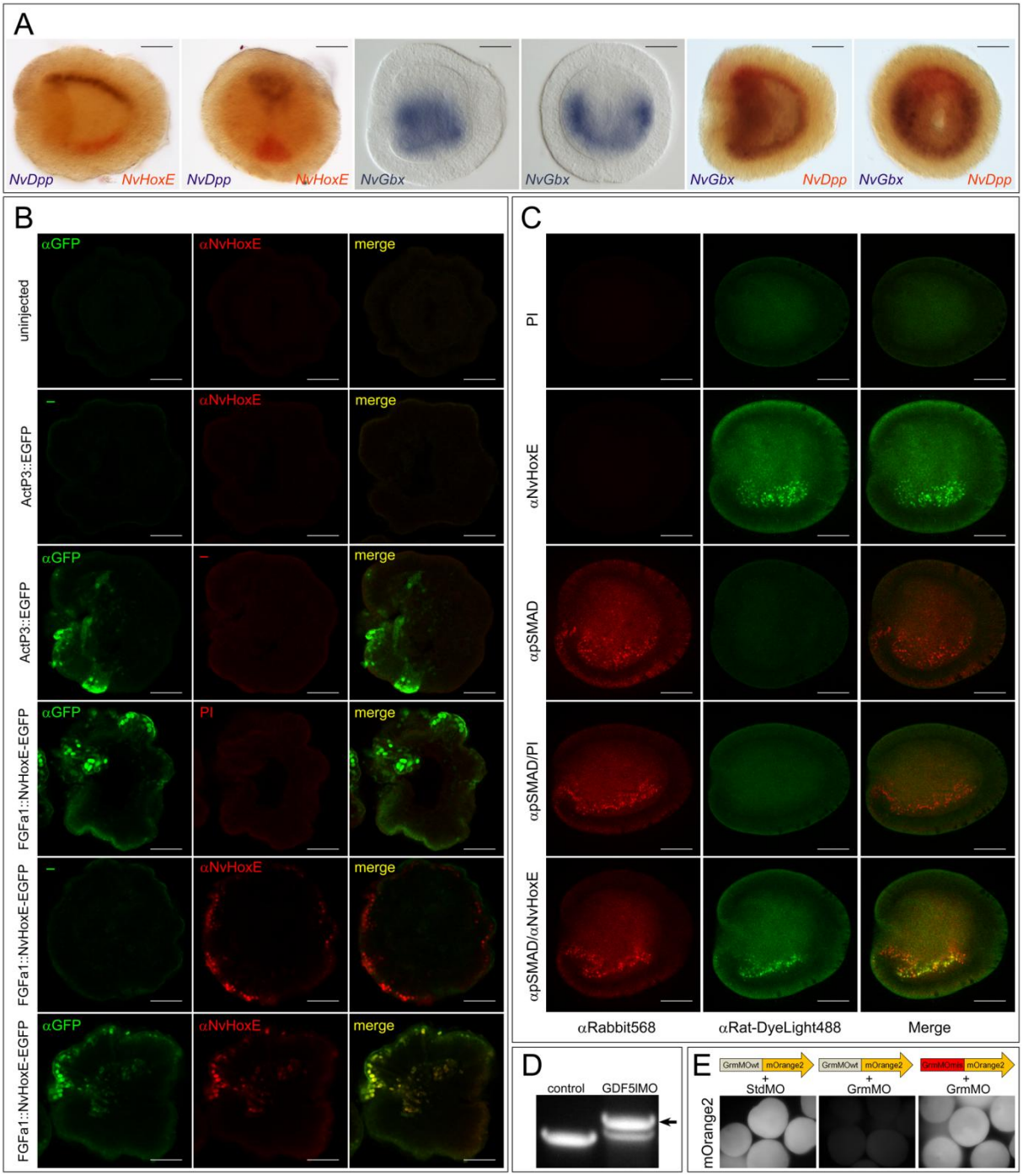

Figure S1 – related to Figure1. Controls for the determination of the BMP signaling side.

(A) *NvDpp* and *NvHoxE* are expressed on the opposing ends of the directive axis in early planula; *NvGbx* is expressed throughout the *NvDpp*-free part of the endoderm.

(B) Anti-NvHoxE antibody specifically stains NvHoxE. All stainings performed at gastrula stage, when no endogenous NvHoxE is expressed. Transgenic ActP3::EGFP - embryos mosaicly expressing EGFP under *Nematostella β-actin* promoter in a subset of cells. Transgenic FGFa1::NvHoxE-EGFP - embryos mosaicly expressing NvHoxE-EGFP fusion protein under *Nematostella FGFa1* promoter in a subset of cells. Both, anti-rat-DyLight549 and anti-rabbit-Alexa488 secondary antibodies were added to each sample. Primary antibodies are marked on the image. Minus sign stands for no primary antibody added. Uninjected embryos are not stained by either anti-GFP or anti-NvHoxE. EGFP expressing embryos are stained only by anti-GFP antibody and not by anti-NvHoxE antibody. NvHoxE-GFP expressing embryos stain with both anti-GFP and anti-NvHoxE antibody and do not stain with rat pre-immune serum (PI).

(C) Anti-NvHoxE antibody specifically stains endodermal nuclei on the pSMAD-positive side of the embryo. Combinations of the primary and secondary antibodies are marked. PI – rat preimmune serum.

(D) Injection of the GDF5lMO results in the retention of an intron with several stop codons in all reading frames in the majority of the *NvGDF5-like* transcripts as revealed by RT PCR. Arrow points at a PCR product containing an intron.

(E) GrmMO specifically inhibits the translation of the target mRNA with a fully complementary recognition sequence and not the one carrying 5 mismatches. Early planulae injected with the in vitro transcribed mRNA carrying the wild type recognition site for GrmMO (GrmMOwt) followed by *mOrange2* sequence are stronlgy fluorescent if co-injected with StdMO but not if co-injected with GrmMO. Early planulae co-injected with mRNA carrying the recognition site for GrmMO with 5 mismatches (GrmMOmis) followed by *mOrange2* sequence are strongly fluorescent and not affected by GrmMO.

Scale bars 50 μm.

Figure S2 - related to Figure 2.

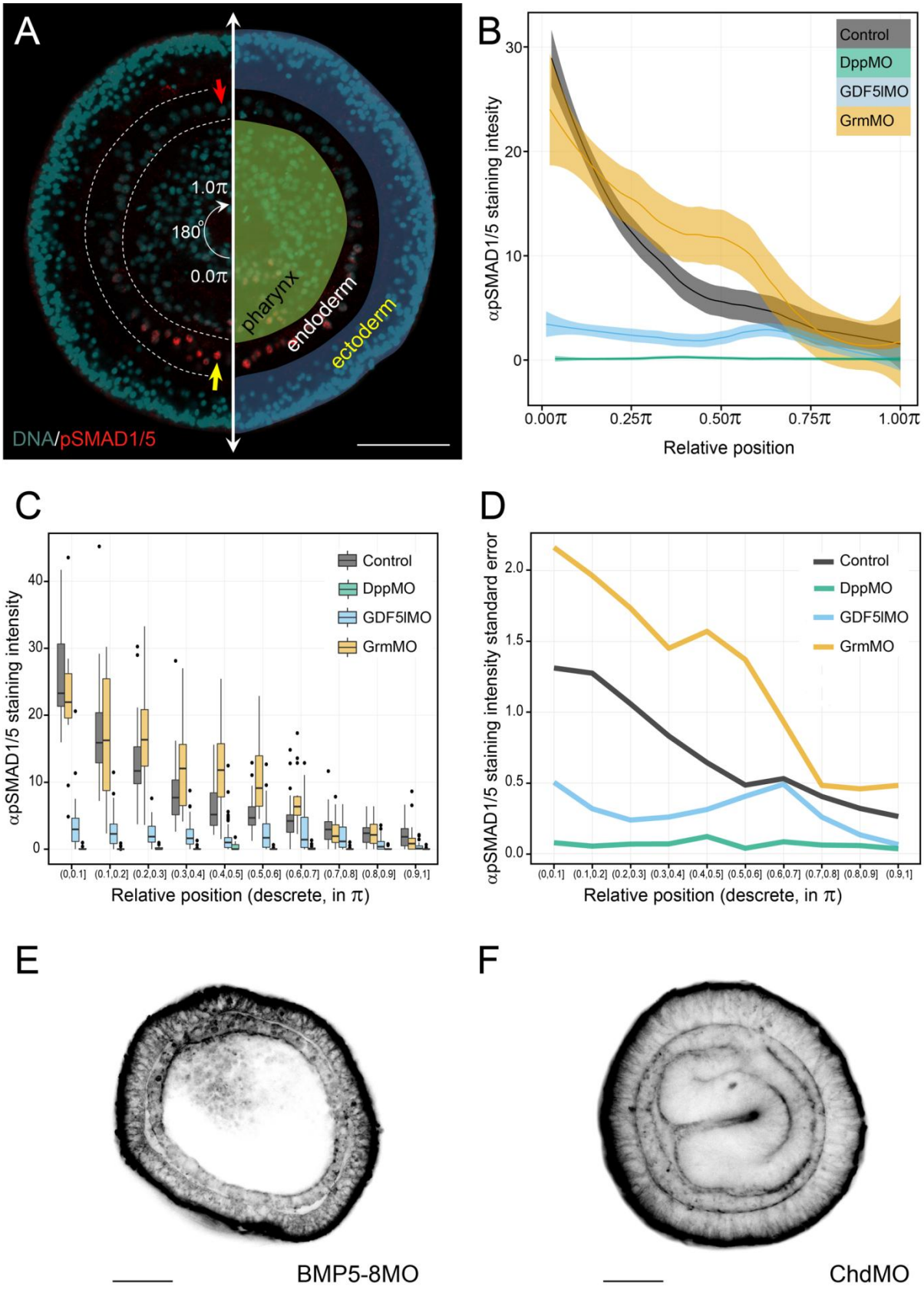

Figure S2, related to Figure 2. Statistical analysis of the BMP signaling gradient and the morphology of the BMP5-8MO and ChdMO late planulae.

(A) The αpSMAD1/5 staining intensity was measured along the arc of 180^0 in the body wall endoderm nuclei (between dashed white lines). The first nucleus to be measured (yellow arrow) is located closest to the centre of the intensively pSMAD1/5-positive domain; the last nucleus to be measured is located at the opposite side of the embryo (red arrow).

(B) αpSMAD1/5 staining intensity as a function of relative position (represented as fraction of the 180^0 arc) along the endoderm perimeter, described by a LOESS smoothed curve (solid line) with a 99% confidence interval for the mean (shade) based on individual measurements from multiple embryos for Control (n=12), GrmMO (n=7), GDF5lMO (n=10), and DppMO (n=8). Relative position allows compensating for different numbers of nuclei in different embryos and gives each nucleus its coordinate. It corresponds to the sequential number of each nucleus divided by total number of endodermal nuclei along the 180^0 arc in the particular embryo (as in A).

(C) pSMAD1/5 staining intensity as a function of relative position along the endoderm perimeter (represented as fractions of the 180^0 arc from 0 to π) in ten equally sized discrete windows, with box plots representing measurements from multiple embryos for Control (n=12), GrmMO (n=7), GDF5lMO (n=10), and DppMO (n=8). The pSMAD1/5 intensity was significantly higher in GrmMO than Control ($p<0.05$, Wilcoxon exact test) in the bins in the range (0.2,0.7]. The pSMAD1/5 intensity was significantly lower ($p<0.01$, Wilcoxon exact test) in GDF5lMO and DppMO treated embryos compared to Control in all positional bins.

(D) Bootstrap estimate of the standard error (SE) for pSMAD1/5 staining intensity for Control (N=12), GrmMO (N=7), GDF5lMO (N=10), and DppMO (N=8) treated embryos as a function of relative position along the endoderm perimeter (represented as fractions of the 180^0 arc) in equally sized discrete windows. The SE for pSMAD1/5 intensity is significantly higher in GrmMO than Control ($p<0.01$, F test) in the bins in the range (0.4,0.6]. A comparison of the residuals in linear model fits of pSMAD1/5 staining intensity to

logarithmic and linear independent variables representing relative position showed that globally, the variance is significantly higher for the GrmMO treated embryos than Control (p-value = 6.893e-07, F test).

(E-F) Oral views of the BMP5-8MO and ChdMO late planulae stained with fluorescent phalloidin. Morphants do not show any sign of mesentery formation.

Scale bars 50 µm.

Figure S3 - related to Figures 3 and 4.

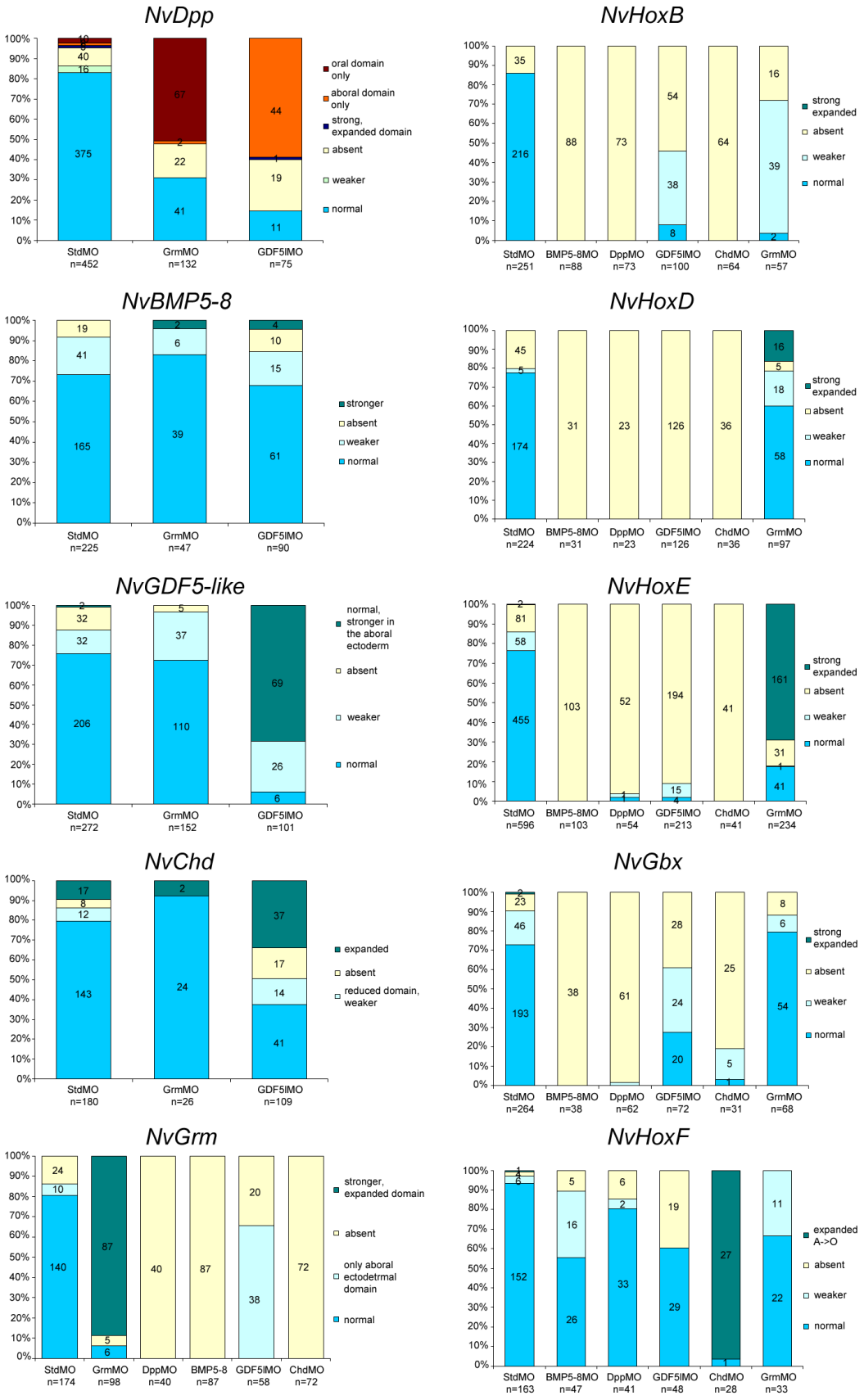

Figure S3 - related to Figures 3 and 4. Penetrance of the morpholino phenotypes

Penetrance of the morpholino phenotypes for the morpholino/gene combinations not reported in (Saina et al., 2009).

Figure S4 - related to Figure 4.

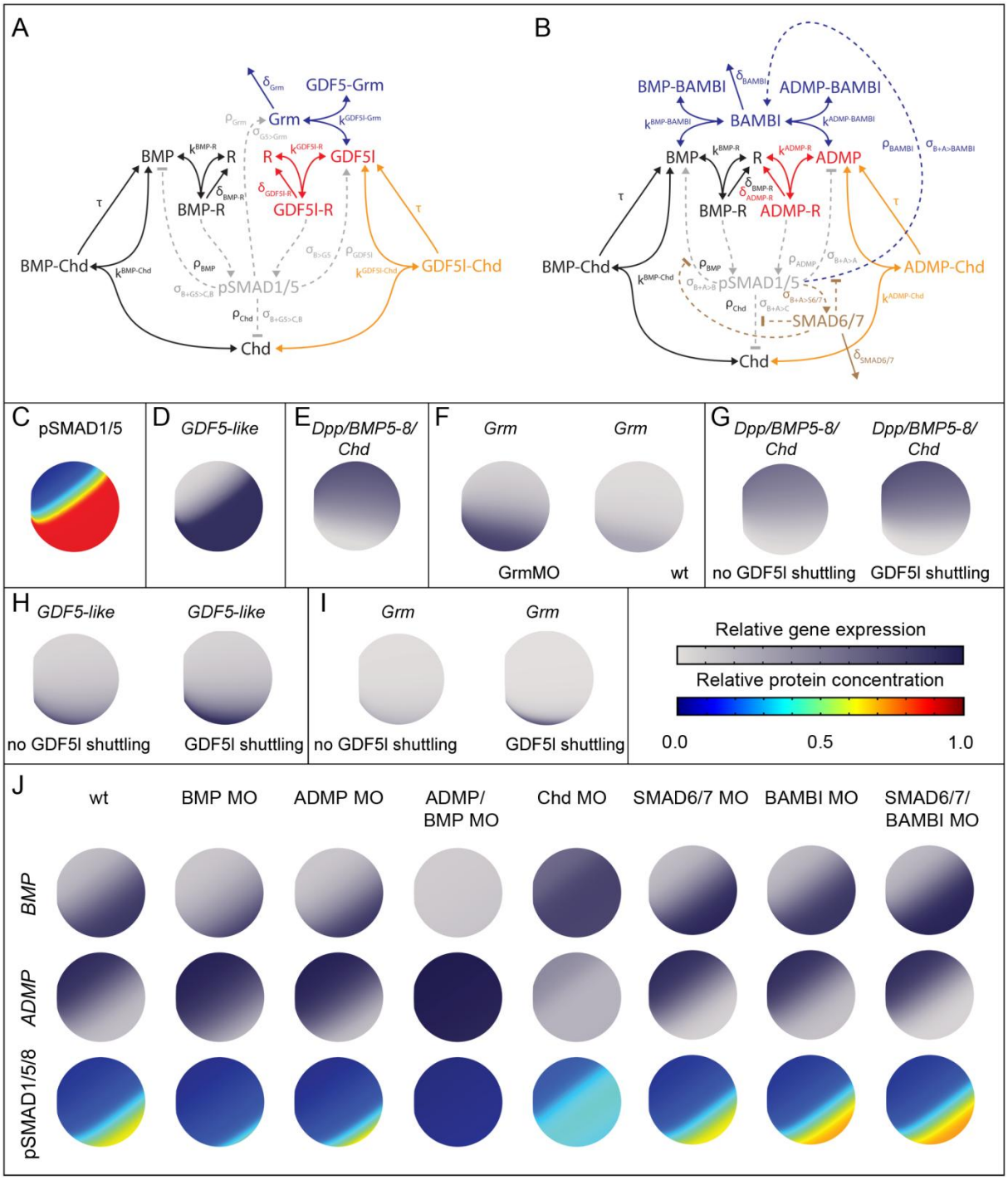

Figure S4 - related to Figure 4. The regulatory interactions of the *Nematostella* and *Xenopus* models.

A-B The regulatory interactions of the core *Drosophila* model (Mizutani et al., 2005) (black arrows) and the model extensions specific for *Nematostella* (A, coloured arrows) and *Xenopus* (B, coloured arrows). Parameter names are written next to the interactions they belong to.

pSMAD1/5 (grey) is included for clarity but was not modelled explicitly. The parameter name above the arrows from pSMAD1/5 to the targets indicates which ligand-receptor complex impacts on the downstream components. Note that in the *Nematostella* model some regulatory interactions only depend on one of the two ligand-receptor complexes, while in *Xenopus* BMP-R and ADMP-R have the same targets.

(C-I) Impact of the sequential incorporation of signalling modules in the *Nematostella* network. Parameter values are as in the standard model, with parameter values of non-incorporated parts set to zero.

(C) The core model (black arrows) results in a stable BMP signaling domain opposite to the *NvChd* expression domain. This domain corresponds to the *NvGDF5-like* expressing domain (D).

(E) Including the negative feedback of both GDF5l-Receptor and BMP-Receptor signaling on BMP and Chordin expression into the model results in the restriction of both the *NvDpp*, *NvBMP5-8* and the *NvChd* expression domains.

(F) Adding NvGrm as an antagonist of NvGDF5-like into the model results in the upregulation of *NvGrm* expression in the NvGrmMO compared to wild type.

(G-I) Shuttling of NvGDF5-like, although not essential, sharpens the expression domains of *BMP* and *NvChd* (G) , *NvGDF5-like* (H) and *NvGrm* (I) compared to the alternative model where only NvDpp/NvBMP5-8 is allowed to shuttle.

(J) Xenopus model. Simulation of the *BMP4/BMP7* (*BMP*) and *ADMP/BMP2* (*ADMP*) mRNA expression patterns and pSMAD1/5/8 localization in wild type and upon knockdown of different BMP network components in *Xenopus*. Relative expression (shown in colour code as ISH) and relative pSMAD1/5 concentrations (shown as heat maps) are plotted onto the Brachet's cleft.

Figure S5 - related to Figure 5

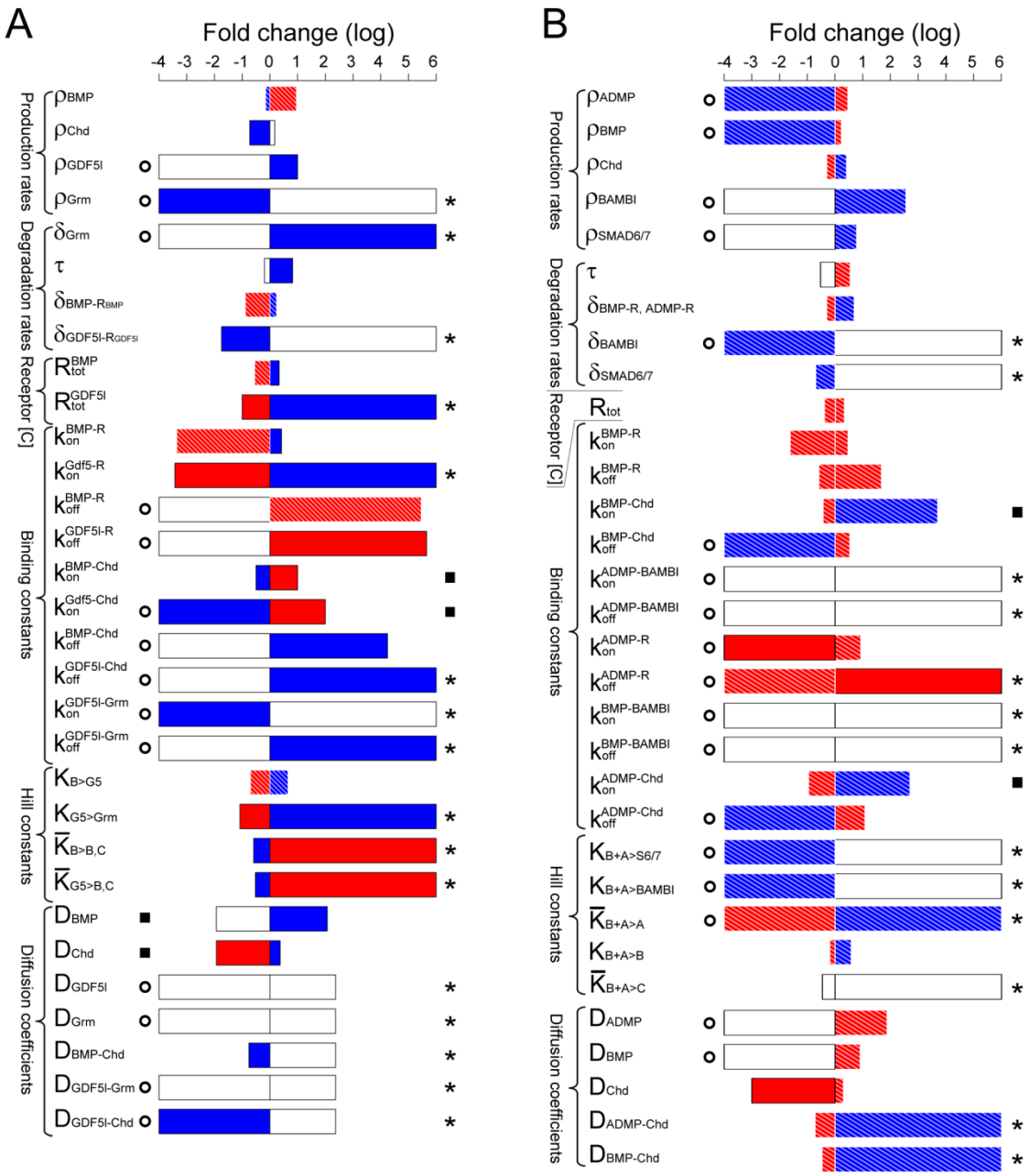

Figure S5 - related to Figure 5. Sensitivity of the asymmetric BMP signaling pattern to the parameter values in the *Nematostella* (A) and *Xenopus* (B) model.

For each parameter, as indicated at the bottom of each bar, we report the relative fold change from the standard value used in the model (indicated by zero) on a logarithmic scale that still permits the emergence of an asymmetric BMP signaling pattern as defined in the Supporting Information. For parameter values outside the bar, asymmetric BMP signaling becomes

symmetric or unstable in that it oscillates over time. A zero at the bottom of the bar indicates that an asymmetric BMP signaling is observed even when the parameter value is set to zero, i.e. when the reaction is absent from the model. A star at the top of a bar indicates that asymmetric BMP signaling was still observed at very large parameter values (infinite values cannot be tested in a simulation framework). A filled square indicates that wider parameter spaces could not be tested due to numerical limitations. Red bars indicate stronger asymmetric BMP signaling; blue bars indicate weaker asymmetric BMP signaling. Red-white bars indicate a shift of the asymmetric BMP signaling domain towards the *NvChd* expression domain in the case of *Nematostella* (A) or a ventralization in the case of the frog (B); blue-white bars indicate a shift in the opposite direction away from the *NvChd* expression domain (A) or a dorsalization (B). White bars indicate that none of these changes in the asymmetric BMP signaling pattern are observed as the parameter values are changed.

Supplemental tables

Table S1, related to Figure 1. TGFβ molecules and BMP antagonists found in *Nematostella vectensis*

Gene name	Accession numbers	Suggested homologues in Bilateria	Asymmetric expression	Knockdown phenotype	References
NvDpp	AY391716 AY363391	*BMP2/4, decapentaplegic*	Yes, at symmetry break	Radialization of *NvDpp*, *NvBMP5-8* and *NvChd*; disappearance of pSMAD1/5; expression of *NvGDF5-like*, *NvGrm*, *Hox* genes and *NvGbx* is abolished	(Finnerty et al., 2004; Rentzsch et al., 2006a; Saina et al., 2009) This paper
NvBMP5-8	DQ358699	*BMP5-8, Screw*	Yes, at symmetry break	Radialization of *NvDpp*, *NvBMP5-8* and *NvChd* expression; disappearance of pSMAD1/5; expression of *NvGDF5-like*, *NvGrm*, *Hox* genes and *NvGbx* is abolished	(Matus et al., 2006b; Saina et al., 2009) This paper
NvGDF5-like	AY496945, AY391717	*Gdf5, Gdf6*	Yes, at symmetry break	Expansion of *NvChd*; reduction of pSMAD1/5; expression of *NvGrm*, *Hox* genes and *NvGbx* is abolished or repressed	(Rentzsch et al., 2006a; Technau et al., 2005) This paper
mstn/gdf11	KC662373	*myostatin, Gdf8/11*	No	N/A	(Saina and Technau, 2009)
NvActivin	ABF61781	*activin*	No	N/A	(Matus et al., 2006a)
NvAdmp-related	JQ959545	*ADMP*	N/A after symmetry	N/A	(Röttinger et al., 2012)

			break		
NvChd	DQ286294 DQ358700	*Chordin, short gastrulation (sog)*	Yes, at symmetry break	Radialization of *NvChd*, disappearance of pSMAD1/5, disappearance of expression of *NvDpp*, *NvBMP5-8*, *NvGDF5-like*, *NvGrm*, *Hox* genes and *NvGbx*	(Matus et al., 2006b; Rentzsch et al., 2006a; Saina et al., 2009) This paper
NvGremlin	DQ517924	*Gremlin*	No	N/A	(Matus et al., 2006a)
NvGrm	DQ471325	*Gremlin*	Yes, at symmetry break	Delay in symmetry break; expansion of pSMAD1/5; expansion of the *NvGrm* and *NvHoxE* expression	(Rentzsch et al., 2006a) This paper
NvFollistatin-like	DQ517921	*Follistatin*	No	N/A	(Matus et al., 2006a)
NvFollistatin	DQ517920	*Follistatin*	No	N/A	(Matus et al., 2006a)
NvNoggin1	DQ517922	*Noggin*	Yes, after symmetry break	N/A	(Matus et al., 2006a)
NvNoggin2	DQ517923	*Noggin*	No	N/A	(Matus et al., 2006a)

N/A – data not available

Table S2, related to Figure 3. Different nomenclature of the *Nematostella vectensis Hox* genes with confirmed expression

This study	Chourrout et al., 2006 (Chourrout et al., 2006)	Ryan et al., 2007 (Ryan et al., 2007)
NvHoxA	*NvHoxA*	*Anthox6*
NvHoxB	*NvHoxB*	*Anthox6a*
NvHoxC	*NvHoxC*	*Anthox7*
*NvHoxD**	*NvHoxDa*	*Anthox8a*
	NvHoxDb	*Anthox8b*
NvHoxE	*NvHoxE*	*Anthox1a*
NvHoxF	*NvHoxF*	*Anthox1*

* *NvHoxDa* and *NvHoxDb* have been shown to be different transcripts originating from the same locus by alternative splicing (Moran et al., 2014). In this study, we name this gene *NvHoxD*.

Supplemental Experimental Procedures

1. Morpholino injection and generating the constitutively active NvBMPRI.

Morpholino oligonucleotides were injected at following concentrations: DppMO (GTAAGAAACAGCGTAAGAGAAGCAT), BMP5-8MO (GTAACAGGTCTCGTATTCTCCGCAT) and ChdMO (GATCCACTCACCATCTTTGCGAGAC) at 300µM concentration as in (Saina et al., 2009) (see also for controls of MO specificity); GDF5LMO (AGGTTATTTAGCCTGACCTTGATCG), GrmMO (CTCAACAGCTTCTTCAATGATCCGT) and standard control morpholino StdMO (CCTCTTACCTCAGTTACAATTTATA) - at 500µM concentration. The functionality of the GDF5lMO was assessed by PCR on cDNA from GDF5l morphants and control embryos (Fig. S1D) followed by sequencing the PCR products; the specificity of the GrmMO, which is constructed against a region in the 5' UTR of the *NvGrm*, was tested by co-injecting mRNA carrying either a wild type sequence (ACGGATCATTGAAGAAGCTGTTGAG) recognized by GrmMO or the one with 5 mismatches (ACTGATGATTGACGAAGTTGTTAAG) upstream of the *mOrange2* coding sequence with StdMO and GrmMO (Fig. S1E). *Nematostella BMPRI* sequence (KJ948110) was mutated by template switching PCR to substitute the Q209 residue by a D residue in the resulting protein to generate a constitutively active BMPRI (Wieser et al., 1995). Then NvBMPRIQ_{209}>D sequence was fused through a Gly4Ser spacer to the EGFP coding sequence and cloned downstream of the 3.4 kb *NvFGFa1* promoter, which has an early ubiquitous activity and drives mosaic transgene expression in the early F0 embryos. Microinjection of the plasmid was carried out as described in (Renfer et al., 2010).

2. NvHoxE protein expression, antibody production, staining and imaging

NvHoxE coding sequence was cloned downstream of the GST and His-tag coding sequence in a pET21 vector. The protein was expressed in Rosetta™(DE3)pLysS Competent Cells (Novagen) and isolated under native conditions on a GSTrap column (GE Healthcare) using the BioRad BioLogic DuoFlow FPLC machine. The tags were cleaved off by AcTEV protease (Invitrogen) according to the manufacturer's protocol, and isolated GST-His tag was trapped from the solution with Ni-NTA agarose (Qiagen). The sequence of the purified protein was confirmed by MSMS. The rat anti-NvHox antibody was produced at BioGenes (Berlin, Germany). The specificity of the antibody (Fig. S1B) was assayed by transiently expressing the NvHoxE-EGFP fusion protein under control of the 3.4 kb *NvFGFa1* promoter, and performing the staining with the anti-NvHoxE and anti-GFP antibodies at the gastrula stage (when endogenous *NvHoxE* is not yet expressed). Embryos injected with EGFP coding sequence downstream of the 1.1 kb *ActP3 Nvβ-actin* promoter were used as control.

For whole mount antibody staining, the embryos were fixed in 4% MEM/PFA containing 0.2% Tween 20 and 0.2% TritonX100 for 30 minutes, then washed 5 times for 5 minutes in 1xPBS containing 0.2% Tween 20 and 0.2% TritonX100 (PBSTT) and blocked in a 4:1 mixture of 1%BSA/PBSTT and heat inactivated sheep serum for 2 hours. The rat anti-NvHoxE antibody (1:500), the rabbit anti-Phospho-Smad1 (Ser463/465)/ Smad5 (Ser463/465)/ Smad8 (Ser426/428) antibody (Cell Signaling, 9511) (1:100), rabbit anti-GFP antibody (abcam, ab290) (1:1000) and mouse anti-GFP antibody (Life Technologies, A11120) (1:500) were preabsorbed in the blocking solution for the time of the blocking. The embryos were stained with primary antibodies overnight at 4^0 and then washed 5 times for 25 minutes with PBSTT at room temperature. The secondary antibody staining and washing was done in the same way as described for the primary antibody. The following secondary antibodies were used: goat anti-rabbit-Alexa Fluor 568 (Life Technologies, A11011), goat anti-rabbit-Alexa Fluor 488 (Life Technologies, A11008), goat anti-rabbit-Alexa Fluor 633

(Life Technologies, A21070), goat anti-rat DyLight549 (Jackson, 112-505-143), goat anti-rat DyLight488 (Rockland, 612-141-120). For imaging, embryos were embedded in Vectashield (Vector Labs). Confocal imaging was done with a Leica TCS SP5X. *In situ* images were taken with Nikon DS-Fi1 camera attached to Nikon Eclipse 80i microscope. Image processing was done in Adobe Photoshop CS5.

3. Quantification of the pSMAD1/5 gradient

Intensity of αpSMAD1/5 staining was quantified on 16 bit images of confocal optical sections (oral views) of early morphant and control planulae stained with DAPI and αpSMAD1/5. Staining intensities of all endodermal nuclei along an arc of 180^0 starting from the centre of the pSMAD1/5-positive domain were collected in ImageJ. Nuclei were detected based on DAPI staining. Each counted nucleus was given a sequential number. To correct for the different numbers of endodermal nuclei in different planulae, the sequential number of each counted nucleus was divided by a total number of counted nuclei on the optical section resulting in a relative position of the nucleus along the 180^0 arc (from 0 to π). Background staining values were calculated for each embryo by measuring and averaging αpSMAD1/5 staining intensity in several endodermal positions, which did not overlap with nuclei. These average background values were subtracted from all the staining intensities prior to analysis. No additional normalization of the data was performed.

4. Mathematical Model

Since the BMP signaling network involves multiple players and the interactions are very complex, a number of mathematical models have been proposed to explain various aspects of D-V patterning (Ben-Zvi et al., 2008; Eldar et al., 2002; Inomata et al., 2013; Lee et al., 2009; Mizutani et al., 2005; Paulsen et al., 2011; Shimmi et al., 2005; Umulis et al., 2006; Umulis et al., 2010) . Yet, to date, there is no mechanistic understanding of the BMP signaling networks outside Bilateria. In our paper, we combine loss of function experiments and mathematical modelling to understand the general rules of BMP signaling-dependent axis patterning in animals.

4.1 Model of directive axis patterning in *Nematostella*

Towards the end of gastrulation two striking events occur: a symmetry break in the expression domains and the emergence of the BMP signaling domain at the opposite site of the *NvDpp* expression domain. To explain the emergence of this counterintuitive signaling pattern of BMP from the asymmetric expression patterns we built a mathematical model for axis patterning in *Nematostella* that is based on the known regulatory interactions between the key regulatory proteins NvDpp/NvBMP5-8/NvGDF5-like, the BMP receptor, the BMP antagonists Chordin (NvChd) and Gremlin (NvGrm), and the protease Tolloid (Figure S7A). The regulatory proteins that have been identified in *Nematostella* are strikingly similar to those involved in dorso-ventral patterning in *Drosophila* and the model therefore builds on a previously published shuttling mechanism for *Drosophila* (Iber and Gaglia, 2007; Mizutani et al., 2005). Since *NvDpp* and *NvBMP5-8* are co-expressed in *Nematostella* and their morpholino phenotypes are indistinguishable (Saina et al., 2009), we assume in the model that NvDpp and NvBMP5-8 heterodimerize to form NvDpp/NvBMP5-8 complex. Interestingly,

heterodimers of *Drosophila* Dpp/Screw and vertebrate BMP4/BMP7 signal stronger (Shimmi et al., 2005; Suzuki et al., 1997) and are shuttled by Chordin preferentially over homodimers (Shimmi et al., 2005).

As a starting point of the model, we mimicked the situation after the symmetry break and, therefore, restricted the expression of NvChd in the initial time steps until the regulatory network can self-maintain the asymmetric expression patterns. After gastrulation, *NvDpp* and *NvBMP5-8* are expressed in a stripe in the endoderm, while *NvChd* remains expressed in the overlying ectoderm, separated by the mesogloea, the extracellular matrix separating ectoderm and endoderm. Although so far, we could not directly show the secretion site of the corresponding proteins, our knockdown experiments suggest that their diffusion and physical interactions most likely occur in the mesogloea, similar to the situation in the frog (Plouhinec et al., 2013). We therefore simplified the geometry by modelling only the mesogloea. As a result, we did not distinguish between the endodermal expression of *NvDpp* and *NvBMP5-8* and the ectodermal expression of *NvChd*, but rather considered NvDpp, NvBMP5-8 and NvChd to be co-produced and co-secreted in the same domain. In doing so, we generated a minimal viable model demonstrating the system of the BMP signaling gradient maintenance in *Nematostella* planula.

4.1.1 Geometry

The geometry of this early developmental stage is similar in *Drosophila* and *Nematostella* in that the embryo is a spherical structure with a diameter of about 200 μm, and in both cases the proteins can diffuse in a fluid-filled cavity (periviteline fluid and mesogloea respectively). In *Drosophila* it surrounds a 1-layered epithelium that secretes the proteins into this space and which harbours the receptors; in case of *Nematostella*, it is sandwiched between two protein secreting 1 cell thick cell layers: the ectoderm on the outside and the endoderm on the inside.

The oral opening can be described as a small interruption in the ectodermal and endodermal cell sheets. In the simplest approximation we can use a 1-dimensional domain with an approximate length of 500 μm and periodic boundary conditions at the ends of the domain. In the more realistic 3-dimensional model, based on measurements of the dimensions of multiple embryos, we represent the mesogloea as the surface of a hollow sphere with a radius of 80 μm and an oral opening of radius 45 μm at one side of the sphere. In this case we use zero flux boundary conditions at the oral pole.

4.1.2 Regulatory interactions

The model for axis patterning in *Nematostella* (Figure S5A) is an adaptation of the model by Mizutani and co-workers for Drosophila (Iber and Gaglia, 2007; Mizutani et al., 2005). The original model for dorso-ventral patterning in *Drosophila* included Dpp ligand, the Dpp ligand-receptor complex, Sog, Tsg, the Sog/Tsg complex, and the Sog/Tsg/Ligand complex. There is no homologue of Tsg in *Nematostella*, and we therefore modified the original model in that we removed Tsg and allowed the heterodimeric NvDpp/NvBMP5-8 ligand (henceforth called BMP) to bind the Sog-homologue Chordin directly without binding of additional proteins, which was shown to be possible in vertebrates(Rentzsch et al., 2006b). In summary, the *Nematostella* model has four components: the Dpp/BMP5-8 ligand (BMP), the ligand-receptor complex (BMP-R), Chordin (Chd), and the Dpp/BMP5-8-Chd complex (BMP-Chd). All components can diffuse at speed D, resulting in a set of reaction-diffusion equations of the form

$$\frac{\partial c_i}{\partial t} = D\Delta c_i + \mathcal{R}(c_i)$$

As the receptor is bound to the surface and cannot diffuse the differential equation for the ligand-receptor complex (BMP-R) reads

$$\frac{\partial[BMP-R]}{\partial t} = \mathcal{R}(BMP-R)$$

The biological processes are translated into the following reaction terms

$$\mathcal{R}(BMP) = \rho_{BMP}\,\Lambda_{BMP}(x) - k_{on}^{BMP-Chd}\,c_{BMP}\,c_{Chd} + \left(k_{off}^{BMP-Chd} + \tau\right)c_{BMP-Chd}$$
$$- k_{on}^{BMP-R}(R_{tot} - c_{BMP-R})\,c_{BMP} + k_{off}^{BMP-R}\,c_{BMP-R}$$
$$\mathcal{R}(BMP-R) = k_{on}^{BMP-R}\,(R_{tot} - c_{BMP-R})c_{BMP} - (k_{off}^{BMP-R} + \delta_{BMP-R})\,c_{BMP-R}$$
$$\mathcal{R}(Chd) = \rho_{Chd}\,\Lambda_{Chd}(x) - k_{on}^{BMP-Chd}\,c_{BMP}\,c_{Chd} + k_{off}^{BMP-Chd}\,c_{BMP-Chd}$$
$$\mathcal{R}(BMP-Chd) = k_{on}^{BMP-Chd}\,c_{BMP}\,c_{Chd} - (k_{off}^{BMP-Chd} + \tau)\,c_{BMP-Chd}$$

The model has been described in detail before (Iber and Gaglia, 2007; Mizutani et al., 2005). In brief, the total BMP receptor concentration R_0 is assumed to be constant over time and space, such that $R_{tot} = c_{BMP-R} + c_R$. The expression of BMP is spatially restricted according to $\Lambda_{BMP}(x)$. BMP-receptor binding and unbinding occurs at rate k_{on}^{BMP-R} and k_{off}^{BMP-R}, respectively. Upon BMP-receptor binding, the ligand is endocytosed and degraded at rate $\delta_{BMP\text{-}R}$, which has been determined experimentally for *Drosophila* embryos. In *Nematostella*, BMP can bind at rate $k_{on}^{BMP-Chd}$ to Chordin, and the BMP-Chordin complex, BMP-Chd, can then dissociate at rate $k_{off}^{BMP-Chd}$. Chordin is expressed in a restricted part of the domain according to $\Lambda_{Chd}(x)$ and can be cleaved by the protease Tolloid at rate τ when bound to the BMP ligand.

As motivated in the main text, in the 3D model we further included the signaling protein NvGDF5-like (GDF5l) and its receptor, as well as Gremlin (Grm), an antagonist of GDF5l. GDF5l is a member of the BMP family, and we therefore allow it to bind to Chordin with the same kinetics as the BMP ligand, i.e. binding at rate $k_{on}^{GDF5l-Chd}$ and unbinding at rate $k_{off}^{GDF5l-Chd}$. Gremlin is a GDF5l antagonist much as Chordin, but it is not cleaved by Tolloid.

We therefore allow it to bind to Gdf5 at the same rate as Chordin, i.e. binding at rate $k_{on}^{GDF5l-Grm}$ and unbinding at rate $k_{off}^{GDF5l-Grm}$. GDF5l expression is induced by BMP-receptor signaling, while Gremlin expression is induced by GDF5l. Both GDF5l and BMP signalling can inhibit Chordin and BMP expression. This translates into the following reaction terms:

$$\mathcal{R}(BMP) = \rho_{BMP}\,\bar{\sigma}_{G5>B,C}\bar{\sigma}_{B>B,C} - k_{on}^{BMP-Chd}\,c_{BMP}\,c_{Chd} + \left(k_{off}^{BMP-Chd} + \tau\right)c_{BMP-Chd} - k_{on}^{BMP-R}\left(R_{tot}^{BMP} - c_{BMP-R}\right)c_{BMP} + k_{off}^{BMP-R}\,c_{BMP-R}$$

$$\mathcal{R}(BMP-R) = k_{on}^{BMP-R}\left(R_{tot}^{BMP} - c_{BMP-R}\right)c_{BMP} - (k_{off}^{BMP-R} + \delta_{BMP-R})\,c_{BMP-R}$$

$$\mathcal{R}(Chd) = \rho_{Chd}\,\Lambda(x,t) - k_{on}^{BMP-Chd}\,c_{BMP}\,c_{Chd} - k_{on}^{GDF5l-Chd}\,c_{GDF5l}\,c_{Chd} + k_{off}^{BMP-Chd}\,c_{BMP-Chd} + k_{off}^{GDF5l-Chd}\,c_{GDF5l-Chd}$$

$$\mathcal{R}(BMP-Chd) = k_{on}^{BMP-Chd}\,c_{BMP}\,c_{Chd} - (k_{off}^{BMP-Chd} + \tau)\,c_{BMP-Chd}$$

$$\mathcal{R}(GDF5l) = \rho_{GDF5l}\,\sigma_{B>G5} - k_{on}^{GDF5l-Chd}\,c_{GDF5l}\,c_{Chd} + (k_{off}^{GDF5l-Chd} + \tau)\,c_{GDF5l-Chd} - k_{on}^{GDF5l-R}\,(R_{tot}^{GDF5l} - c_{GDF5l-R1})\,c_{GDF5l} + k_{off}^{GDF5l-R}\,c_{GDF5l-R1} - k_{on}^{GDF5l-Grm}\,c_{GDF5l}\,c_{Grm} + k_{off}^{GDF5l-Grm}\,c_{Grm-GDF5l}$$

$$\mathcal{R}(GDF5l-R) = k_{on}^{GDF5l-R}\left(R_{tot}^{GDF5l} - c_{GDF5l-R1}\right)c_{GDF5l} - (k_{off}^{GDF5l-R} + \delta_{GDF5l-R1})\,c_{GDF5l-R1}$$

$$\mathcal{R}(GDF5l-Chd) = k_{on}^{GDF5l-Chd}\,c_{GDF5l}\,c_{Chd} - (k_{off}^{GDF5l-Chd} + \tau)\,c_{GDF5l-Chd}$$

$$\mathcal{R}(Grm) = \rho_{Grm}\sigma_{G5>Grm} - \delta_{Grm}c_{Grm} - k_{on}^{GDF5l-Grm}\,c_{Grm}\,c_{GDF5l} + k_{off}^{GDF5l-Grm}\,c_{Grm-GDF5l}$$

$$\mathcal{R}(Grm-GDF5l) = k_{on}^{GDF5l-Grm}\,c_{Grm}\,c_{GDF5l} - k_{off}^{GDF5l-Grm}\,c_{Grm-GDF5l}$$

4.1.3 Parameter Values

<u>1D model:</u>

The parameter values are the same as previously (Iber and Gaglia, 2007; Mizutani et al., 2005), with exception of the Tolloid activity, τ, which we lowered about 10-fold compared to the previous model, to compensate for the removal of Tsg.

Parameter	**Value**	**Explanation**	**Ref**
ρ_{BMP}	0.001 μM s^{-1}	Production rate BMP	(Iber and Gaglia, 2007;

			Mizutani et al., 2005)
ρ_{Chd}	0.08 μM s^{-1}	Production rate Chd	(Iber and Gaglia, 2007; Mizutani et al., 2005)
R_{tot}	3 μM	Concentration of BMP receptor	(Iber and Gaglia, 2007; Mizutani et al., 2005)
$k_{on}^{BMP-Chd}$	95 μM^{-1} s^{-1}	Binding rate of BMP to Chordin	(Iber and Gaglia, 2007; Mizutani et al., 2005)
$k_{off}^{BMP-Chd}$	$4*10^{-6}$ s^{-1}	Unbinding rate of the BMP-Chd complex	(Iber and Gaglia, 2007; Mizutani et al., 2005)
k_{on}^{BMP-R}	0.4 μM^{-1} s^{-1}	Binding rate of BMP to its receptor	(Iber and Gaglia, 2007; Mizutani et al., 2005)
k_{off}^{BMP-R}	$4*10^{-6}$ s^{-1}	Unbinding rate of the BMP-receptor complex	(Iber and Gaglia, 2007; Mizutani et al., 2005)
δ_{BMP-R}	$5*10^{-4}$ s^{-1}	Degradation rate of BMP-receptor complex	(Iber and Gaglia, 2007; Mizutani et al., 2005)

τ	0.05 s^{-1}	Tolloid-mediated degradation rate of BMP-Chd complexes	
D	85 μm^2 s^{-1}	Diffusion coefficient of BMP, Chd and BMP-Chd complex	(Iber and Gaglia, 2007; Mizutani et al., 2005)
L	500 μm	Length of the 1D domain	measured

The production of Chordin is restricted to parts of the domain, using

$$\Lambda_{Chd}(x) = \begin{cases} 1 & \text{if} \quad 0 < x < \frac{\pi}{2} \quad \vee \quad \frac{3\pi}{2} < x < 2\pi \\ 0 & \text{if} \quad \frac{\pi}{2} < x < \frac{3\pi}{2} \end{cases}$$

As we investigate the effects of three different BMP expression domains three different values are assigned to $\Lambda_{BMP}(x)$:

$\Lambda_{BMP}(x) = \Lambda_{Chd}(x)$ if BMP expression is on the same site as Chordin expression.

$\Lambda_{BMP}(x) = 1 - \Lambda_{Chd}(x)$ if BMP expression is on the opposite site as Chordin expression.

$\Lambda_{BMP}(x) = \frac{1}{2}$ if BMP expression homogeneous.

3D model:

The parameter values are the same as in the 1D model unless otherwise indicated in the Ref column. The constants without an entry in the Ref column were adjusted to match the observed expression patterns.

Parameter	Value	Explanation	Ref
ρ_{BMP}	0.001 μM s^{-1}	Production rate BMP	(Iber and Gaglia, 2007; Mizutani et al., 2005)
ρ_{Chd}	0.08 μM s^{-1}	Production rate Chd	(Iber and Gaglia, 2007; Mizutani et al., 2005)
ρ_{GDF5l}	0.001 μM s^{-1}	Production rate GDF5l	Assumed to be the equal to ρ_{BMP}
ρ_{Grm}	0.003 μM s^{-1}	Production rate Grm	
δ_{Grm}	0.001 s^{-1}	Degradation rate Grm	
τ	0.05 s^{-1}	Tolloid-mediated degradation rate of Ligand-Chd complexes	Same as in 1D model
$\delta_{BMP\text{-}R}$	$5*10^{-4}$ s^{-1}	Degradation rate of BMP-receptor complex	(Iber and Gaglia, 2007; Mizutani et al., 2005)
$\delta_{GDF5l\text{-}R1}$	$5*10^{-4}$ s^{-1}	Degradation rate of GDF5l-receptor complex	Assumed to be equal to $\delta_{BMP\text{-}R}$
R_{tot}^{BMP}	3 μM	Concentration of BMP receptor	(Iber and Gaglia, 2007; Mizutani et al., 2005)
R_{tot}^{GDF5l}	3 μM	Concentration of GDF5l receptor	Assumed to be equal to R_{tot}^{BMP}
k_{on}^{BMP-R}	0.4 μM^{-1} s^{-1}	Binding rate of BMP to its receptor	(Iber and Gaglia, 2007;

			Mizutani et al., 2005)
$k_{on}^{\mathrm{GDF5l}-R}$	0.4 μM^{-1} s^{-1}	Binding rate of GDF5l to its receptor	Assumed to be equal to k_{on}^{BMP-R}
k_{off}^{BMP-R}	$4*10^{-6}$ s^{-1}	Unbinding rate of the BMP-receptor complex	(Iber and Gaglia, 2007; Mizutani et al., 2005)
$k_{off}^{\mathrm{GDF5l}-R}$	$4*10^{-6}$ s^{-1}	Unbinding rate of the GDF5l-receptor complex	Assumed to be equal to k_{off}^{BMP-R}
$k_{on}^{BMP-Chd}$	95 μM^{-1} s^{-1}	Binding rate of BMP to Chordin	(Iber and Gaglia, 2007; Mizutani et al., 2005)
$k_{on}^{\mathrm{GDF5l}-Chd}$	95 μM^{-1} s^{-1}	Binding rate of GDF5l to Chordin	Assumed to be equal to $k_{on}^{BMP-Chd}$
$k_{off}^{BMP-Chd}$	$4*10^{-6}$ s^{-1}	Unbinding rate of the BMP-Chd complex	(Iber and Gaglia, 2007; Mizutani et al., 2005)
$k_{off}^{\mathrm{GDF5l}-Chd}$	$4*10^{-6}$ s^{-1}	Unbinding rate of the GDF5l-Chd complex	Assumed to be equal to $k_{off}^{BMP-Chd}$
$k_{on}^{\mathrm{GDF5l}-Grm}$	95 μM^{-1} s^{-1}	Binding rate of GDF5l to Gremlin	Assumed to be equal to $k_{on}^{BMP-Chd}$
$k_{off}^{GDF5l-Grm}$	$4*10^{-6}$ s^{-1}	Unbinding rate of the GDF5l-Gremlin complex	Assumed to be

			equal to $k_{off}^{BMP-Chd}$
$K_{B>G5}$	1 μM	Activating Hill constant of the BMP-R complex	
$K_{G5>Grm}$	0.6 μM	Activating Hill constant of the GDF5l-R1 complex	
$\bar{K}_{B>C,B}$	0.5 μM	Inhibiting Hill constant of the BMP-R complex	
$\bar{K}_{G5>C,B}$	0.1 μM	Inhibiting Hill constant of the GDF5l-R1 complex	
D_{BMP}	85 $\mu m^2 s^{-1}$	Diffusion coefficient BMP	(Iber and Gaglia, 2007; Mizutani et al., 2005)
D_{Chd}	85 $\mu m^2 s^{-1}$	Diffusion coefficient Chd	(Iber and Gaglia, 2007; Mizutani et al., 2005)
D_{GDF5l}	85 $\mu m^2 s^{-1}$	Diffusion coefficient GDF5l	Assumed to be equal to all other diffusion constants
D_{Grm}	85 $\mu m^2 s^{-1}$	Diffusion coefficient Grm	Assumed to be equal to all other diffusion constants
$D_{BMP-Chd}$	85 $\mu m^2 s^{-1}$	Diffusion coefficient BMP-Chd complex	(Iber and Gaglia, 2007; Mizutani et al., 2005)
$D_{GDF5l-Grm}$	85 $\mu m^2 s^{-1}$	Diffusion coefficient GDF5l-Grm complex	Assumed to be equal to all other diffusion constants

$D_{GDF5l\text{-}Chd}$	85 $\mu m^2 s^{-1}$	Diffusion coefficient GDF5l-Chd complex	Assumed to be equal to all other diffusion constants
r_{ball}	80 µm	Measured radius of the mesogloea in the embryo	Measured
r_{mouth}	45 µm	Measured radius of the oral opening	Measured

BMP is expressed homogenously, while Chordin is restricted to the following domain:

$$\Lambda(x,t) = \begin{cases} 1.4 * x + z > 110\ \mu m & if\ t \leq 2\ h \\ \bar{\sigma}_{G5>B,C}\ \bar{\sigma}_{B>B,C} & if\ t > 2\ h \end{cases}$$

Activating Hill terms are denoted $\sigma_{C1>C2}$, where C1 is the component that is signaling and thereby inducing the expression of component C2. Inhibiting Hill terms are denoted $\bar{\sigma}_{C1>C2}$, where C1 is the component that is signaling and thereby inhibiting the expression of component C2:

$$\sigma_{C1>C2} = \frac{C1^n}{C1^n + {K_{C1>C2}}^n}$$

and

$$\bar{\sigma}_{C1>C2} = \frac{{\bar{K}_{C1>C2}}^n}{C1^n + {\bar{K}_{C1>C2}}^n}$$

4.2 Model of DV patterning in the Frog

4.2.1 Geometry

The geometry of this early developmental stage is similar, but much larger than in *Nematostella* , in that the embryo is a spherical structure with a radius of about 550 μm. Extracellular proteins can diffuse in the Brachet's cleft, a thin layer of extracellular matrix between ectoderm and endomesoderm (Plouhinec et al., 2013). In our 3-dimensional model, we represent the Brachet's cleft as the surface of a hollow sphere with a radius of 550 μm and a blastopore opening of radius 150 μm on one side of the sphere. We use zero flux boundary conditions at the blastopore opening.

4.2.2 Regulatory interactions

The *Xenopus* model has 6 main components: the BMP4/7 ligand (BMP), the ADMP/BMP2 ligand (ADMP), Chordin (Chd), the BMP/ADMP receptor (R), BAMBI and SMAD6/7. For simplicity, we absorbed the effects of Twisted gastrulation protein, which promotes diffusion of the Chd-BMP complex (Oelgeschlager et al., 2000; Wang et al., 2008), into the parameter values. We also did not model the effects of the important modulators of the Tolloid activity – the dorsally expressed ONT1 (Inomata et al., 2008) and the ventrally expressed Sizzled (Inomata et al., 2013), which keep Tolloid activity highest at intermediate BMP signaling levels, - but rather absorbed them in the Tolloid activity (τ) directly. We did not consider CV2, which is a ventrally expressed protein exhibiting pro-BMP and anti-BMP activities depending on the context (Ambrosio et al., 2008). We also assumed Chordin to be the sole dorsally expressed BMP inhibitor, thus ignoring Noggin and Follistatin (Khokha et al., 2005), which are not regulated by Tolloid cleavage.

In brief, the total BMP/ADMP receptor concentration R_{tot} is assumed to be constant over time and space, such that $R_{tot} = c_{BMP-R} + c_{ADMP-R} + c_R$. Upon BMP-receptor or ADMP-receptor

binding , the ligand is endocytosed and degraded at rate $\delta_{BMP\text{-}R}$ or $\delta_{ADMP\text{-}R}$ respectively. Both BMP and ADMP can bind at rate $k_{on}^{BMP-Chd}$ (Piccolo et al., 1996) and $k_{on}^{ADMP-Chd}$ to Chordin (Reversade and De Robertis, 2005). The BMP-Chordin (BMP-Chd) and ADMP-Chordin complex (ADMP-Chd), can then dissociate at rate $k_{off}^{BMP-Chd}$ and $k_{off}^{ADMP-Chd}$. Chordin is expressed in a restricted part of the domain according to $\Lambda_{Chd}(x)$ and can be cleaved by the protease Tolloid (Lee et al., 2006; Lee et al., 2009) at rate τ when bound to the BMP or ADMP ligand.

We further included a dominant negative BMP receptor BAMBI (Onichtchouk et al., 1999) and inhibitory SMAD6/7 (Imamura et al., 1997; Nakao et al., 1997), which are negative feedback antagonists of BMP/ADMP signaling (Paulsen et al., 2011). Both BMP and ADMP bind to BAMBI at rate $k_{on}^{BMP-BAMBI}$ and $k_{on}^{ADMP-BAMBI}$ and unbind at rate $k_{off}^{BMP-BAMBI}$ and $k_{off}^{ADMP-BAMBI}$. As BAMBI is only a derivative of the BMP receptor, we decided to use the same degradation rates $\delta_{BMP\text{-}R}$ and $\delta_{ADMP\text{-}R}$ for the BMP/ADMP bound BAMBI receptors. Production of SMAD6/7 is induced upon BMP/ADMP signaling and SMAD6/7 inhibits BMP/ADMP signaling by competitive inhibition (Paulsen et al., 2011). Both, ADMP and BMP signaling, inhibit Chordin and ADMP expression, and induce BMP, BAMBI and SMAD6/7 expression (for review see (Plouhinec et al., 2011). This translates into the following reaction terms:

$$\mathcal{R}(BMP) = \rho_{BMP}(0.1 + \sigma_{B+A>B}) - k_{on}^{BMP-Chd} c_{BMP}\, c_{Chd} + (k_{off}^{BMP-Chd} + \tau)\, c_{BMP-Chd} - k_{on}^{BMP-R}(R_{tot} - c_{BMP-R} - c_{ADMP-R})\, c_{BMP} + k_{off}^{BMP-R}\, c_{BMP-R} - k_{on}^{BMP-BAMBI} c_{BMP}\, c_{BAMBI} + k_{off}^{BMP-BAMBI}\, c_{BMP-BAMBI}$$

$$\mathcal{R}(BMP-R) = k_{on}^{BMP-R}(R_{tot} - c_{BMP-R} - c_{ADMP-R}) c_{BMP} - (k_{off}^{BMP-R} + \delta_{BMP-R})\, c_{BMP-R}$$

$$\mathcal{R}(Chd) = \rho_{Chd}\, \Lambda(x) \bar{\sigma}_{B+A>C} - k_{on}^{BMP-Chd} c_{BMP}\, c_{Chd} + k_{off}^{BMP-Chd}\, c_{BMP-Chd} - k_{on}^{ADMP-Chd} c_{ADMP}\, c_{Chd} + k_{off}^{ADMP-Chd}\, c_{ADMP-Chd}$$

$$\mathcal{R}(BMP-Chd) = k_{on}^{BMP-Chd} c_{BMP}\, c_{Chd} - (k_{off}^{BMP-Chd} + \tau)\, c_{BMP-Chd}$$

$$\mathcal{R}(ADMP) = \rho_{ADMP}\, \bar{\sigma}_{B+A>A} - k_{on}^{ADMP-Chd} c_{ADMP}\, c_{Chd} + (k_{off}^{ADMP-Chd} + \tau)\, c_{ADMP-Chd} - k_{on}^{ADMP-R}(R_{tot} - c_{BMP-R} - c_{ADMP-R})\, c_{ADMP} + k_{off}^{ADMP-R}\, c_{ADMP-R} - k_{on}^{ADMP-BAMBI} c_{ADMP}\, c_{Bambi} + k_{off}^{ADMP-BAMBI}\, c_{ADMP-BAMBI}$$

$$\mathcal{R}(ADMP-R) = k_{on}^{ADMP-R}(R_{tot} - c_{BMP-R} - c_{ADMP-R}) c_{ADMP} - (k_{off}^{ADMP-R} + \delta_{ADMP-R})\, c_{ADMP-R}$$

$$\mathcal{R}(ADMP - Chd) = k_{on}^{ADMP-Chd} c_{ADMP}\, c_{Chd} - (k_{off}^{ADMP-Chd} + \tau)\, c_{ADMP-Chd}$$

$$\mathcal{R}(BAMBI) = \rho_{BAMBI}\, \sigma_{B+A>BAMBI} - \delta_{BAMBI}\, c_{BAMBI} - k_{on}^{BMP-BAMBI} c_{BMP}\, c_{BAMBI} + k_{off}^{BMP-BAMBI}\, c_{BMP-BAMBI} - k_{on}^{ADMP-BAMBI} c_{ADMP}\, c_{BAMBI} + k_{off}^{ADMP-BAMBI}\, c_{ADMP-BAMBI}$$

$$\mathcal{R}(BMP - BAMBI) = k_{on}^{BMP-BAMBI} c_{BMP}\, c_{BAMBI} - k_{off}^{BMP-BAMBI}\, c_{BMP-BAMBI} - \delta_{BMP-R}\, c_{BMP-BAMBI}$$

$$\mathcal{R}(ADMP - BAMBI) = k_{on}^{ADMP-BAMBI} c_{ADMP}\, c_{BAMBI} - k_{off}^{ADMP-BAMBI}\, c_{ADMP-BAMBI} - \delta_{ADMP-R}\, c_{ADMP-BAMBI}$$

$$\mathcal{R}(SMAD6/7) = \rho_{SMAD}\, \sigma_{B+A>S6/7} - \delta_{SMAD}\, c_{SMAD6/7}$$

4.2.3 Parameter Values

In contrast to *Nematostella*, some quantitative data is available for *Xenopus*.

1. Spatially averaged Chordin concentration of around 33 nM (Lee et al., 2006)
2. BMP4/BMP7 concentration in the range between 0.1 nM and 2.5 nM (Piccolo et al., 1996)
3. KD value for BMP4/7 and Chd = 3.2 ± 0.6*10-10 M (Piccolo et al., 1996).
4. KD value for BMP4 and BMP receptor = 2.5 – 9 *10-10 M (Graff et al., 1994; Penton et al., 1994).

All the other parameter values were adjusted to obtain the published expression patterns and observe the four measured concentrations and affinities listed above. We note that given the change in the decay rates, also the diffusion coefficients needed to be adjusted. The diffusion coefficients of 85 μm^2/s chosen by Mizutani and co-workers are at the high end of what has been measured for proteins diffusion in tissue (Yu et al., 2009). The new 3.4-fold lower diffusion coefficients are thus if anything more realistic (Kalwarczyk et al., 2012; Muller et al., 2012; Zhou et al., 2012). We note that the model also works over a broad range of parameters closer to the ones used in *Nematostella*. However it would then not observe the measured values above.

Parameter	**Value**	**Explanation**
ρ_{BMP}	$3*10^{-7}$ μM s^{-1}	Production rate BMP

ρ_{Chd}	$1.5*10^{-5}$ μM s^{-1}	Production rate Chd
ρ_{ADMP}	$1*10^{-7}$ μM s^{-1}	Production rate ADMP
ρ_{BAMBI}	$1.8*10^{-6}$ μM s^{-1}	Production rate BAMBI
ρ_{SMAD}	$3*10^{-4}$ μM s^{-1}	Production rate SMAD
τ	0.0017 s^{-1}	Tolloid-mediated degradation rate of Ligand-Chd complexes
$\delta_{BMP\text{-}R}$, $\delta_{ADMP\text{-}R}$	$5*10^{-4}$ s^{-1}	Degradation rate of BMP-receptor / ADMP-receptor complex (as in (Iber and Gaglia, 2007; Mizutani et al., 2005))
δ_{BAMBI}	$1*10^{-3}$ s^{-1}	Degradation rate of BAMBI
δ_{SMAD}	$1*10^{-4}$ s^{-1}	Degradation rate of SMAD6/7
R_{tot}	$1.5*10^{-3}$ μM	Concentration of BMP/ADMP receptor
k_{on}^{BMP-R}	8 μM^{-1} s^{-1}	Binding rate of BMP to its receptor
k_{on}^{ADMP-R}	8 μM^{-1} s^{-1}	Binding rate of ADMP to its receptor
k_{off}^{BMP-R}	$4*10^{-3}$ s^{-1}	Unbinding rate of the BMP-receptor complex
k_{off}^{ADMP-R}	$4*10^{-3}$ s^{-1}	Unbinding rate of the ADMP-receptor complex
$k_{on}^{BMP-Chd}$	14 μM^{-1} s^{-1}	Binding rate of BMP to Chordin
$k_{on}^{ADMP-Chd}$	14 μM^{-1} s^{-1}	Binding rate of ADMP to Chordin
$k_{off}^{BMP-Chd}$	$4.5*10^{-3}$ s^{-1}	Unbinding rate of the BMP-Chd complex
$k_{off}^{ADMP-Chd}$	$4.5*10^{-3}$ s^{-1}	Unbinding rate of the ADMP-Chd complex
$k_{on}^{ADMP-BAMBI}$	8 μM^{-1} s^{-1}	Binding rate of ADMP to BAMBI
$k_{on}^{BMP-BAMBI}$	8 μM^{-1} s^{-1}	Binding rate of BMP to BAMBI
$k_{off}^{ADMP-BAMBI}$	$4*10^{-3}$ s^{-1}	Unbinding rate of the ADMP-BAMBI complex
$k_{off}^{BMP-BAMBI}$	$4*10^{-3}$ s^{-1}	Unbinding rate of the BMP-BAMBI complex
$K_{B+A>B}$	$2.25*10^{-4}$ μM	Activating Hill constant on BMP expression
$K_{B+A>BAMBI}$	$1.5*10^{-3}$ μM	Activating Hill constant on BAMBI expression
$K_{B+A>S6/7}$	$1.5*10^{-3}$ μM	Activating Hill constant on SMAD6/7 expression
$\overline{K}_{B+A>C}$	$7.5*10^{-4}$ μM	Inhibiting Hill constant on Chordin expression

$\bar{K}_{B+A>A}$	$2.25*10^{-4}$ μM	Inhibiting Hill constant on ADMP expression
D_{BMP}	25 $\mu m^2 s^{-1}$	Diffusion coefficient BMP
D_{Chd}	25 $\mu m^2 s^{-1}$	Diffusion coefficient Chd
D_{ADMP}	25 $\mu m^2 s^{-1}$	Diffusion coefficient ADMP
$D_{ADMP\text{-}Chd}$	25 $\mu m^2 s^{-1}$	Diffusion coefficient ADMP-Chd complex
$D_{BMP\text{-}Chd}$	25 $\mu m^2 s^{-1}$	Diffusion coefficient BMP-Chd complex
r_{ball}	550 μm	Radius of the Brachet's cleft in the embryo
$r_{blastopore}$	150 μm	Radius of the blastopore opening

Production of Chordin is restricted to part of the domain, using

$$\Lambda(x) = 1.3 * x + z > 300\ \mu m$$

In the frog model, all Hill terms depend on both ADMP and BMP signaling. This signaling induces SMAD6/7 activation, which acts as a competitive inhibitor. Activating Hill terms are therefore as denoted $\sigma_{B+A>C1}$, where BMP and ADMP are the components that are signaling and thereby inducing the expression component C1. Inhibiting Hill terms are denoted $\bar{\sigma}_{B+A>C1}$, where BMP and ADMP are the components that are signaling and thereby inhibiting the expression of component C1:

$$\sigma_{B+A>C1} = \frac{(c_{BMP-R} + c_{ADMP-R})^n}{(c_{BMP-R} + c_{ADMP-R})^n + (K_{B+A>C1}\,(1 + c_{SMAD6/7}))^n}$$

and

$$\bar{\sigma}_{B+A>C1} = \frac{(\bar{K}_{B+A>C1}\,(1 + c_{SMAD6/7}))^n}{(c_{BMP-R} + c_{ADMP-R})^n + (\bar{K}_{B+A>C1}\,(1 + c_{SMAD6/7}))^n}$$

4.3 Model analysis

4.3.1 Comparison of simulation results with experimental data

Antibody stainings detect proteins, and thus provide a measure of protein concentrations. We therefore compare the antibody stainings to the values of the variables in our model (which represent protein concentrations).

In situ hybridization (ISH) experiments provide a (semi-quantitative) measure of the mRNA concentration, i.e. of the protein expression rate (rather than the protein concentration). To compare ISH results with our simulations, we thus compare them to the production terms in the model (rather than the variables, which would represent concentrations).

4.3.2. Simulation of Morphants

We model Morpholino experiments by reducing the production rates of the relevant proteins. In the *Nematostella* simulations of the Chordin, GDF5l and Gremlin morphants, the production rate was reduced to 10% of the standard values (Table 2). In the BMP morphant we reduced the production rate to 5% of the original value to avoid oscillations.

MO knockdowns in the frog show in general a less extreme phenotype compared to *Nematostella*, possibly due to partial compensation by redundant BMP proteins. In our simulations all knockdowns were therefore modeled by a reduction of the production rates or by setting the Tolloid cleavage rate to 20% of the standard values in order to reproduce the less severe MO effects.

4.3.3 Sensitivity Analysis

We conducted a sensitivity analysis to determine the range of parameter values for which the pattern of interest would be observed. We report an upper and lower boundary for each parameter value; parameter values outside of these boundaries result in a loss of pattern. A key event in the simulation is the emergence of an asymmetric BMP5-8/Dpp signaling pattern in *Nematostella* and the emergence of an asymmetric BMP4/7 signaling pattern in *Xenopus*. Thus, we define the lack of an asymmetric BMP5-8/Dpp or BMP4/7 signaling pattern as a loss of pattern.

In particular, an asymmetric BMP5-8/Dpp signaling pattern is considered absent if one of the following three conditions is met:

1. The maximum of $\sigma_{B>G5}$, the Hill function inducing GDF5l expression, is below 0.3.
2. The ratio between the maximal and minimal GDF5l expression is less than 3-fold.
3. The system is unstable and oscillates.

In the frog, an asymmetric BMP4/7 signaling pattern is considered absent if one of the following three conditions is met:

1. The maximum of $\sigma_{B+A>B}$, the Hill function inducing BMP expression, is below 0.3.
2. The ratio between the maximum and minimum of the Hill function $\sigma_{B+A>B}$ is less than 3-fold.
3. The system is unstable and oscillates.

We further report if increasing or decreasing a parameter value leads to stronger (red) or weaker (blue) expression domains.

In *Nematostella*, in a few cases the *NvGDF5-like* expression domain is expanded while the *NvDpp/NvBMP5-8/NvChd* expression domain is reduced. This results in a shift of the *NvGDF5-like* expression domain towards the *NvChd* expression domain (red with white lines).

The opposite case, a reduced *NvGDF5-like* and an expanded *Dpp/BMP5-8/Chd* expression domain, results in a shift of *NvChd* expression towards the *NvDpp/NvBMP5-8/NvChd* expression domain (blue with white lines).

These cases are similar to dorsalization (blue with white lines) and ventralization (red with white lines) in the frog.

Expansions/Reductions of the expression domains were judged by eye.
In some cases we were not able to increase or decrease the parameter range any further due to numerical problems with the stiff set of equations. These cases are denoted by a filled black square. The results of the sensitivity analysis are presented on Figure S6.

4.4 Materials and methods

The PDEs were solved with finite element methods as implemented in COMSOL Multiphysics 4.3b as previously described (Germann et al., 2011).

Supplemental References

Ambrosio, A.L., Taelman, V.F., Lee, H.X., Metzinger, C.A., Coffinier, C., and De Robertis, E.M. (2008). Crossveinless-2 Is a BMP feedback inhibitor that binds Chordin/BMP to regulate Xenopus embryonic patterning. Dev. Cell *15*, 248-260.

Ben-Zvi, D., Shilo, B.Z., Fainsod, A., and Barkai, N. (2008). Scaling of the BMP activation gradient in Xenopus embryos. Nature *453*, 1205-1211.

Chourrout, D., Delsuc, F., Chourrout, P., Edvardsen, R.B., Rentzsch, F., Renfer, E., Jensen, M.F., Zhu, B., de Jong, P., Steele, R.E., *et al.* (2006). Minimal ProtoHox cluster inferred from bilaterian and cnidarian Hox complements. Nature *442*, 684-687.

Eldar, A., Dorfman, R., Weiss, D., Ashe, H., Shilo, B.Z., and Barkai, N. (2002). Robustness of the BMP morphogen gradient in Drosophila embryonic patterning. Nature *419*, 304-308.

Finnerty, J.R., Pang, K., Burton, P., Paulson, D., and Martindale, M.Q. (2004). Origins of bilateral symmetry: Hox and dpp expression in a sea anemone. Science *304*, 1335-1337.

Germann, P., Menshykau, D., Tanaka, S., and Iber, D. (2011). Simulating Organogensis in COMSOL. In Proceedings of COMSOL Conference 2011 (Stuttgart, COMSOL).

Graff, J.M., Thies, R.S., Song, J.J., Celeste, A.J., and Melton, D.A. (1994). Studies with a Xenopus BMP receptor suggest that ventral mesoderm-inducing signals override dorsal signals in vivo. Cell *79*, 169-179.

Iber, D., and Gaglia, G. (2007). The mechanism of sudden stripe formation during dorso-ventral patterning in Drosophila. J. Math. Biol. *54*, 179-198.

Imamura, T., Takase, M., Nishihara, A., Oeda, E., Hanai, J., Kawabata, M., and Miyazono, K. (1997). Smad6 inhibits signalling by the TGF-beta superfamily. Nature *389*, 622-626.

Inomata, H., Haraguchi, T., and Sasai, Y. (2008). Robust stability of the embryonic axial pattern requires a secreted scaffold for chordin degradation. Cell *134*, 854-865.

Inomata, H., Shibata, T., Haraguchi, T., and Sasai, Y. (2013). Scaling of dorsal-ventral patterning by embryo size-dependent degradation of Spemann's organizer signals. Cell *153*, 1296-1311.

Kalwarczyk, T., Tabaka, M., and Holyst, R. (2012). Biologistics--diffusion coefficients for complete proteome of Escherichia coli. Bioinformatics *28*, 2971-2978.

Khokha, M.K., Yeh, J., Grammer, T.C., and Harland, R.M. (2005). Depletion of three BMP antagonists from Spemann's organizer leads to a catastrophic loss of dorsal structures. Dev. Cell. *8*, 401-411.

Lee, H.X., Ambrosio, A.L., Reversade, B., and De Robertis, E.M. (2006). Embryonic dorsal-ventral signaling: secreted frizzled-related proteins as inhibitors of tolloid proteinases. Cell *124*, 147-159.

Lee, H.X., Mendes, F.A., Plouhinec, J.L., and De Robertis, E.M. (2009). Enzymatic regulation of pattern: BMP4 binds CUB domains of Tolloids and inhibits proteinase activity. Genes Dev. *23*, 2551-2562.

Matus, D.Q., Pang, K., Marlow, H., Dunn, C.W., Thomsen, G.H., and Martindale, M.Q. (2006a). Molecular evidence for deep evolutionary roots of bilaterality in animal development. Proc. Natl. Acad. Sci. USA *103*, 11195-11200.

Matus, D.Q., Thomsen, G.H., and Martindale, M.Q. (2006b). Dorso/ventral genes are asymmetrically expressed and involved in germ-layer demarcation during cnidarian gastrulation. Curr. Biol. *16*, 499-505.

Mizutani, C.M., Nie, Q., Wan, F.Y., Zhang, Y.T., Vilmos, P., Sousa-Neves, R., Bier, E., Marsh, J.L., and Lander, A.D. (2005). Formation of the BMP activity gradient in the Drosophila embryo. Dev. Cell *8*, 915-924.

Moran, Y., Fredman, D., Praher, D., Li, X.Z., Wee, L.M., Rentzsch, F., Zamore, P.D., Technau, U., and Seitz, H. (2014). Cnidarian microRNAs frequently regulate targets by cleavage. Genome Res. *24*, 651-663.

Muller, P., Rogers, K.W., Jordan, B.M., Lee, J.S., Robson, D., Ramanathan, S., and Schier, A.F. (2012). Differential diffusivity of Nodal and Lefty underlies a reaction-diffusion patterning system. Science *336*, 721-724.

Nakao, A., Afrakhte, M., Moren, A., Nakayama, T., Christian, J.L., Heuchel, R., Itoh, S., Kawabata, M., Heldin, N.E., Heldin, C.H., *et al.* (1997). Identification of Smad7, a TGFbeta-inducible antagonist of TGF-beta signalling. Nature *389*, 631-635.

Oelgeschlager, M., Larrain, J., Geissert, D., and De Robertis, E.M. (2000). The evolutionarily conserved BMP-binding protein Twisted gastrulation promotes BMP signalling. Nature *405*, 757-763.

Onichtchouk, D., Chen, Y.G., Dosch, R., Gawantka, V., Delius, H., Massague, J., and Niehrs, C. (1999). Silencing of TGF-beta signalling by the pseudoreceptor BAMBI. Nature *401*, 480-485.

Paulsen, M., Legewie, S., Eils, R., Karaulanov, E., and Niehrs, C. (2011). Negative feedback in the bone morphogenetic protein 4 (BMP4) synexpression group governs its dynamic signaling range and canalizes development. Proc. Natl. Acad. Sci. USA *108*, 10202-10207.

Penton, A., Chen, Y., Staehling-Hampton, K., Wrana, J.L., Attisano, L., Szidonya, J., Cassill, J.A., Massague, J., and Hoffmann, F.M. (1994). Identification of two bone morphogenetic protein type I receptors in Drosophila and evidence that Brk25D is a decapentaplegic receptor. Cell *78*, 239-250.

Piccolo, S., Sasai, Y., Lu, B., and De Robertis, E.M. (1996). Dorsoventral patterning in Xenopus: inhibition of ventral signals by direct binding of chordin to BMP-4. Cell *86*, 589-598.

Plouhinec, J.L., Zakin, L., and De Robertis, E.M. (2011). Systems control of BMP morphogen flow in vertebrate embryos. Curr. Op. Genet. Dev. *21*, 696-703.

Plouhinec, J.L., Zakin, L., Moriyama, Y., and De Robertis, E.M. (2013). Chordin forms a self-organizing morphogen gradient in the extracellular space between ectoderm and mesoderm in the Xenopus embryo. Proc. Natl. Acad. Sci. USA *110*, 20372-20379.

Renfer, E., Amon-Hassenzahl, A., Steinmetz, P.R., and Technau, U. (2010). A muscle-specific transgenic reporter line of the sea anemone, Nematostella vectensis. Proc. Natl. Acad. Sci. USA *107*, 104-108.

Rentzsch, F., Anton, R., Saina, M., Hammerschmidt, M., Holstein, T.W., and Technau, U. (2006a). Asymmetric expression of the BMP antagonists chordin and gremlin in the sea anemone Nematostella vectensis: implications for the evolution of axial patterning. Dev. Biol. *296*, 375-387.

Rentzsch, F., Zhang, J., Kramer, C., Sebald, W., and Hammerschmidt, M. (2006b). Crossveinless 2 is an essential positive feedback regulator of Bmp signaling during zebrafish gastrulation. Development *133*, 801-811.

Reversade, B., and De Robertis, E.M. (2005). Regulation of ADMP and BMP2/4/7 at opposite embryonic poles generates a self-regulating morphogenetic field. Cell *123*, 1147-1160.

Röttinger, E., Dahlin, P., and Martindale, M.Q. (2012). A Framework for the Establishment of a Cnidarian Gene Regulatory Network for "Endomesoderm" Specification: The Inputs of ss-Catenin/TCF Signaling. PLoS Genet. *8*, e1003164.

Ryan, J.F., Mazza, M.E., Pang, K., Matus, D.Q., Baxevanis, A.D., Martindale, M.Q., and Finnerty, J.R. (2007). Pre-bilaterian origins of the Hox cluster and the Hox code: evidence from the sea anemone, Nematostella vectensis. PLoS ONE *2*, e153.

Saina, M., Genikhovich, G., Renfer, E., and Technau, U. (2009). BMPs and chordin regulate patterning of the directive axis in a sea anemone. Proc. Natl. Acad. Sci. USA *106*, 18592-18597.

Saina, M., and Technau, U. (2009). Characterization of myostatin/gdf8/11 in the starlet sea anemone Nematostella vectensis. J. Exp. Zool. B., Mol. Dev. Evol. *312*, 780-788.

Technau, U., Rudd, S., Maxwell, P., Gordon, P.M., Saina, M., Grasso, L.C., Hayward, D.C., Shimmi, O., Umulis, D., Othmer, H., and O'Connor, M.B. (2005). Facilitated transport of a Dpp/Scw heterodimer by Sog/Tsg leads to robust patterning of the Drosophila blastoderm embryo. Cell *120*, 873-886.

Sensen, C.W., Saint, R., Holstein, T.W., *et al.* (2005). Maintenance of ancestral complexity and non-metazoan genes in two basal cnidarians. Trends Genet *21*, 633-639.

Suzuki, A., Kaneko, E., Maeda, J., and Ueno, N. (1997). Mesoderm induction by BMP-4 and -7 heterodimers. Biochem. Biophys. Res. Com.*232*, 153-156.

Umulis, D.M., Serpe, M., O'Connor, M.B., and Othmer, H.G. (2006). Robust, bistable patterning of the dorsal surface of the Drosophila embryo. Proc. Natl. Acad. Sci. USA *103*, 11613-11618.

Umulis, D.M., Shimmi, O., O'Connor, M.B., and Othmer, H.G. (2010). Organism-scale modeling of early Drosophila patterning via bone morphogenetic proteins. Dev. Cell *18*, 260-274.

Wang, X., Harris, R.E., Bayston, L.J., and Ashe, H.L. (2008). Type IV collagens regulate BMP signalling in Drosophila. Nature *455*, 72-77.

Wieser, R., Wrana, J.L., and Massague, J. (1995). GS domain mutations that constitutively activate T beta R-I, the downstream signaling component in the TGF-beta receptor complex. EMBO J. *14*, 2199-2208.

Yu, S.R., Burkhardt, M., Nowak, M., Ries, J., Petrasek, Z., Scholpp, S., Schwille, P., and Brand, M. (2009). Fgf8 morphogen gradient forms by a source-sink mechanism with freely diffusing molecules. Nature *461*, 533-536.

Zhou, S., Lo, W.C., Suhalim, J.L., Digman, M.A., Gratton, E., Nie, Q., and Lander, A.D. (2012). Free extracellular diffusion creates the Dpp morphogen gradient of the Drosophila wing disc. Curr. Biol. *22*, 668-675.